Table 2A

Name	Accession	iTRAQ peptides	Unused	%Cov	Entrez Gene Name(Human homolog)	Symbol (Human)	Entrez GENE ID (Human)
Prolactin	gi|185132553	115	29.9	79.04999852	Prolactin	PRL	5617
Similar to Granzyme-like protein 1 precursor (GLP-1)	gi|189535255	1	1.84	11.11000031	Granzyme B (granzyme 2, cytotoxic T-lymphocyte-associated serine esterase 1)	GZMB	3002
Prolactin II	gi|41019311	8	1.53	36.10999882			
26S proteasome non-ATPase regulatory subunit 4	gi|209736020	1	2.02	11.14000008	Proteasome (prosome, macropain) 26S subunit, non-ATPase, 4	PSMD4	5710
Heterogeneous nuclear ribonucleoprotein A1	gi|223647288	9	31.63	68.22999716	Heterogeneous nuclear ribonucleoprotein A1	HNRNPA1	3178
Unnamed protein product	gi|47222767	1	2.09	9.316000342	Rho guanine nucleotide exchange factor (GEF) 19	ARHGEF19	128272
Melanin-concentrating hormone precursor	gi|213457	17	5.52	53.7899971	Pro-melanin-concentrating hormone	PMCH	5367
Proopiomelanocortine A	gi|185132704	20	8.51	32.01999962	Proopiomelanocortin	POMC	5443
Proopiomelanocortin	gi|530904	7	2	46.90000117	Proopiomelanocortin	POMC	5443
Isotocin / neurophysin 1 precursor	gi|418825	12	5.7	13.2100001	Arginine vasopressin	AVP	551
Unnamed protein product	gi|47219657	1	2.02	12.88000047	Ubiquitin specific peptidase 7 (herpes virus-associated)	USP7	7874
Clathrin light chain A	gi|209731460	1	2.06	33.32999945	Clathrin, light chain A	CLTA	1211
Unnamed protein product	gi|47230642	11	11.91	28.74000072	Secretogranin III	SCG3	29106
PHD finger protein 17	gi|41054211	1	1.71	7.117000222	PHD finger protein 17	PHF17	79960
60 kDa heat shock protein, mitochondrial precursor	gi|209153200	2	6.41	20.20999938	Heat shock 60kDa protein 1 (chaperonin)	HSPD1	3329
S100-B [Salmo salar]	gi|226443324	1	4	38.94999921	S100 calcium binding protein B	S100B	6285
ATP synthase H+ transporting mitochondrial F1 complex beta	gi|198285477	89	45.41	75.34999847	ATP synthase, H+ transporting, mitochondrial F1 complex, beta polypeptide	ATP5B	506
Myosin light chain 2	gi|7678750	1	1.81	11.76000014	Myosin light chain, phosphorylatable, fast skeletal muscle	MYLPF	29895
Actin-related protein 2/3 complex subunit 5	gi|223647102	1	2.02	20.0000003	Actin related protein 2/3 complex, subunit 5, 16kDa	ARPC5	10092
Tubulin beta-3 chain	gi|213514092	3	2.1	47.87999988	Tubulin, beta 3	TUBB3	10381
Mitochondrial import receptor subunit TOM22 homolog	gi|225707812	1	2	9.701000154	Translocase of outer mitochondrial membrane 22 homolog (yeast)	TOMM22	56993
NADP-dependent malic enzyme, mitochondrial precursor	gi|223647696	1	2	3.582999855	Malic enzyme 3, NADP(+)-dependent, mitochondrial	ME3	10873
Tubulin alpha chain	gi|267071	2	2	70.95000148	Tubulin, alpha 1c	TUBA1C	84790
Unnamed protein product	gi|47212864	2	1.85	6.173000112	Myosin XVIIIA	MYO18A	399687
Hypothetical protein	gi|164518348	1	1.52	3.458999842	Orofacial cleft 1 candidate 1	OFCC1	266553
Proteasome subunit beta type 2	gi|225705784	1	2.05	23.49999994	Proteasome (prosome, macropain) subunit, beta type, 2	PSMB2	5690
Creatine kinase B-type	gi|213513714	34	24.21	71.39000297	Creatine kinase, brain	CKB	1152
Vacuolar ATP synthase catalytic subunit A	gi|224587380	1	2	47.27999866	ATPase, H+ transporting, lysosomal 70kDa, V1 subunit A	ATP6V1A	523

Sept2 protein	gi|94574481	1	2.01	10.39000005	Septin 2	SEPT2	4735
Similar to restin	gi|189524793	1	1.7	10.44000015	CAP-GLY domain containing linker protein 1	CLIP1	6249
Neuromodulin	gi|213513358	1	3.17	19.28000003	Growth associated protein 43	GAP43	2596
DnaJ homolog subfamily C member 3	gi|213510886	1	1.4	12.20000014	DnaJ (Hsp40) homolog, subfamily C, member 3	DNAJC3	5611
Unnamed protein product	gi|47228465	1	4.1	29.31999862	Heterogeneous nuclear ribonucleoprotein D (AU-rich element RNA binding protein 1, 37kDa)	HNRNPD	3184
Hyperosmotic glycine rich protein-like	gi|198285593	10	12.58	75.62999725	Cold inducible RNA binding protein	CIRBP	1153
Unnamed protein product	gi|47218197	1	2.21	9.765999764	Calcium/calmodulin-dependent protein kinase II gamma	CAMK2G	818
Small nuclear ribonucleoprotein-associated protein B	gi|213512296	1	2.01	27.00000107	Small nuclear ribonucleoprotein polypeptide N	SNRPN	6638
Glyceraldehyde-3-phosphate dehydrogenase	gi|225715600	1	4.01	32.73000121	Glyceraldehyde-3-phosphate dehydrogenase	GAPDH (includes EG:2597)	2597
4-aminobutyrate aminotransferase, mitochondrial precursor	gi|209154560	1	1.58	15.19999951	4-aminobutyrate aminotransferase	ABAT	18
Aldolase a, fructose-bisphosphate 1	gi|213511774	1	3.74	43.79999936	Aldolase C, fructose-bisphosphate	ALDOC	230
Unnamed protein product	gi|47216776	1	2	14.49999958	Vacuolar protein sorting 29 homolog (S. cerevisiae)	VPS29	51699
Novel protein similar to human general control of amino-acid synthesis 1-like 1	gi|33284844	1	1.45	4.444999993	GCN1 general control of amino-acid synthesis 1-like 1 (yeast)	GCN1L1	10985
60S ribosomal protein L24	gi|209731598	1	2.91	15.28999954	Ribosomal protein L24	RPL24	6152
Triosephosphate isomerase	gi|209734404	46	12.25	53.22999954	Triosephosphate isomerase 1	TPI1	7167
Proprotein convertase subtilisin/kexin type 1	gi|212549686	1	2.95	9.66899991	Proprotein convertase subtilisin/kexin type 1	PCSK1	5122
Hemoglobin subunit beta	gi|209735786	1	2.18	95.27000189	Hemoglobin, beta	HBB (includes EG:3043)	3043
Prothymosin alpha	gi|221221610	4	10	44.13999915	Prothymosin, alpha	PTMA	5757
Unnamed protein product	gi|47222619	1	2.58	9.464000165	Apoptosis-inducing factor, mitochondrion-associated, 1	AIFM1	9131
Alpha-globin 4	gi|162949430	23	15.96	62.94000149	Hemoglobin, alpha 2	HBA2	3040
Hemoglobin subunit beta-1	gi|225703790	48	24.03	89.80000019	Hemoglobin, gamma A	HBG1	3047
Calreticulin	gi|185134556	8	36.38	60.61999798	Calreticulin	CALR	811
Unnamed protein product	gi|47214161	1	1.73	20.6400007	Enoyl CoA hydratase domain containing 2	ECHDC2	55268
SMEK homolog 2	gi|223647852	1	1.74	6.795000285	SMEK homolog 2, suppressor of mek1 (Dictyostelium)	SMEK2	57223
Unnamed protein product	gi|47203923	2	2	6.168999895	Actin filament associated protein 1-like 2	AFAP1L2	84632
Gonadotrophin alpha 1 subunit	gi|546258	18	8.22	63.02999854	Glycoprotein hormones, alpha polypeptide	CGA	1081
Follicle stimulating hormone beta subunit	gi|45685133	5	6.8	29.19999957	Follicle stimulating hormone, beta polypeptide	FSHB	2488
Hypothetical protein LOC335859	gi|189526442	1	2.03	4.540000111	Fatty acid synthase	FASN	2194
Dynactin subunit 2	gi|209155422	5	5.97	23.2099995	Dynactin 2 (p50)	DCTN2	10540
Melanin concentrating hormone 2 (MCH2) precursor	gi|213455	16	5.82	41.67000055	Pro-melanin-concentrating hormone	PMCH	5367
60S acidic ribosomal protein P2	gi|225703274	1	3.85	57.88999796	Ribosomal protein, large, P2	RPLP2	6181
Rho GDP-dissociation inhibitor 1	gi|209154488	5	5.18	36.75999939	Rho GDP dissociation inhibitor (GDI) alpha	ARHGDIA	396
Hypothetical protein LOC569455	gi|224496028	1	1.42	4.828000069	Importin 5	IPO5	3843
Growth hormone 2	gi|159032827	40	23.93	87.13999987	Growth hormone 1	GH1	2688
Somatolactin (alpha)	gi|134726	74	27.38	64.38000202			

Table 2B

Name	Fold Change	StDev	PVal	EF	Lower CI	Upper CI	Location	Type(s)
	GH1-treated / Non-treated	GH1-treated / Non-treated	GH1-treated / Non-treated	GH1-treated / Non-treated	GH1-treated / Non-treated	GH1-treated / Non-treated		
Prolactin	2.290868044	0.011725673	0.002106669	1.270573974	1.803017974	5.915616989	Extracellular space	Cytokine
Similar to Granzyme-like protein 1 precursor (GLP-1)	1.870682001		0.349433392	2.089296103	0.895364821	3.944572926	Cytoplasm	Peptidase
Prolactin II	1.853531957	0.02704107	0.42510739	1.202263951	1.541700006	2.355048895		
26S proteasome non-ATPase regulatory subunit 4	1.803017974		0.367049694	2.089296103	0.862978518	3.80189395	Cytoplasm	Other
Heterogeneous nuclear ribonucleoprotein A1	1.721868992	0.089899039	0.497172803	1.614359021	1.066596031	6.08134985	Nucleus	Other
Unnamed protein product	1.599557996		0.435547709	2.089296103	0.765596628	3.372873068	unknown	Other
Melanin-concentrating hormone precursor	1.584892988	0.066547362	0.428161502	1.342764974	1.180320978	2.582259893	Extracellular space	Other
Proopiomelanocortine A	1.55596602	0.016729234	0.672467113	1.180320978	1.318256974	2.089296103	Extracellular space	Other
Proopiomelanocortin	1.541700006	0.063988531	0.562245309	1.472311974	1.047129035	2.703958035	Extracellular space	Other
Isotocin / neurophysin 1 precursor	1.527565956	0.039493514	0.617341816	1.355188966	1.127197981	3.66437602	Extracellular space	Other
Unnamed protein product	1.499685049		0.482902408	2.108628035	0.711213529	3.133285999	Nucleus	Peptidase
Clathrin light chain A	1.445440054		0.513746679	2.108628035	0.685488224	3.019952059	Plasma membrane	Other
Unnamed protein product	1.432188034	0.069806954	0.367831409	1.432188034	1	2.630268097	Extracellular space	Other
PHD finger protein 17	1.380383968		0.549392521	2.089296103	0.660693526	2.91071701	Nucleus	Other
60 kDa heat shock protein, mitochondrial precursor	1.367728949	0.014446496	0.394513786	2.089296103	0.654636085	2.85758996	Cytoplasm	Enzyme
S100-B [Salmo salar]	1.367728949		0.558983624	2.089296103	0.654636085	2.884032011	Cytoplasm	Other
ATP synthase H+ transporting mitochondrial F1 complex beta	1.355188966	0.024410988	0.04585408	1.14815402	1.180320978	1.584892988	Cytoplasm	Transporter
Myosin light chain 2	1.355188966		0.56853348	2.089296103	0.648634374	2.83139205	Cytoplasm	Other
Actin-related protein 2/3 complex subunit 5	1.342764974		0.575936973	2.089296103	0.642687678	2.83139205	Cytoplasm	Other
Tubulin beta-3 chain	1.330453992	0.037739066	0.53627342	1.419057012	0.937561989	1.887990952	Cytoplasm	Other
Mitochondrial import receptor subunit TOM22 homolog	1.330453992		0.58843261	2.089296103	0.636795521	2.779712915	Cytoplasm	Transporter
NADP-dependent malic enzyme, mitochondrial precursor	1.318256974		0.601977408	2.108628035	0.625172675	2.754229069	Cytoplasm	Enzyme
Tubulin alpha chain	1.318256974	0.023815861	0.575083613	2.089296103	0.630957425	2.779712915	Cytoplasm	Other
Unnamed protein product	1.318256974	0.051703542	0.535494089	2.089296103	0.630957425	2.779712915	Cytoplasm	Other
Hypothetical protein	1.30617094		0.605844915	2.089296103	0.625172675	2.728977919	unknown	Other
Proteasome subunit beta type 2	1.29419601		0.62100333	2.108628035	0.613762021	2.703958035	Cytoplasm	Peptidase
Creatine kinase B-type	1.28233099	0.040311887	0.324288607	1.235947013	1.037528038	1.737800956	Cytoplasm	Kinase
Vacuolar ATP synthase catalytic subunit A	1.28233099		0.625988781	2.089296103	0.613762021	2.703958035	Cytoplasm	Transporter
Sept2 protein	1.28233099		0.626250029	2.089296103	0.613762021	2.703958035	Cytoplasm	Enzyme

Similar to restin	1.270573974		0.644315183	2.108628035	0.602559626	2.654606104	Cytoplasm	Other
Neuromodulin	1.258924961		0.650084972	2.089296103	0.602559626	2.630268097	Plasma membrane	Other
DnaJ homolog subfamily C member 3	0.794328213		0.667952716	2.089296103	0.376703799	1.659587026	Cytoplasm	Other
Unnamed protein product	0.794328213		0.674318373	2.089296103	0.380189389	1.659587026	Nucleus	Transcription regulator
Hyperosmotic glycine rich protein-like	0.787045777	0.041524451	0.524631321	1.247382998	0.591561615	0.981747925	Nucleus	Other
Unnamed protein product	0.787045777		0.657890975	2.089296103	0.373250186	1.644371986	Cytoplasm	Kinase
Small nuclear ribonucleoprotein-associated protein B	0.779830098		0.650910974	2.089296103	0.373250186	1.629295945	Nucleus	Other
Glyceraldehyde-3-phosphate dehydrogenase	0.765596628		0.629889786	2.089296103	0.366437614	1.599557996	Cytoplasm	Enzyme
4-aminobutyrate aminotransferase, mitochondrial precursor	0.758577585		0.622181296	2.108628035	0.363078088	1.599557996	Cytoplasm	Enzyme
Aldolase a, fructose-bisphosphate 1	0.758577585		0.61985302	2.108628035	0.363078088	1.599557996	Cytoplasm	Enzyme
Unnamed protein product	0.758577585		0.620348215	2.108628035	0.363078088	1.599557996	Cytoplasm	Transporter
Novel protein similar to human general control of amino-acid synthesis 1-like 1	0.751622915		0.608968377	2.089296103	0.359749287	1.570363045	Cytoplasm	Translation regulator
60S ribosomal protein L24	0.731139123		0.58094883	2.108628035	0.349945188	1.541700006	Cytoplasm	Other
Triosephosphate isomerase	0.731139123	0.020682539	0.375185192	1.16949904	0.515228629	0.855066717	Cytoplasm	Enzyme
Proprotein convertase subtilisin/kexin type 1	0.717794299		0.565635085	2.108628035	0.343558013	1.51356101	Extracellular space	Peptidase
Hemoglobin subunit beta	0.711213529		0.548802316	2.089296103	0.337287307	1.485936046	Cytoplasm	Transporter
Prothymosin alpha	0.691830993	0.041728616	0.526520073	1.419057012	0.373250186	0.981747925	Nucleus	Transcription regulator
Unnamed protein product	0.685488224		0.515590072	2.089296103	0.325087309	1.432188034	Cytoplasm	Enzyme
Alpha-globin 4	0.679203629	0.130065185	0.892440081	1.472311974	0.405508488	1	Cytoplasm	Transporter
Hemoglobin subunit beta-1	0.679203629	0.029096079	0.370831192	1.224616051	0.165958703	0.831763685	Cytoplasm	Transporter
Calreticulin	0.660693526	0.087643152	0.574053884	1.584892988	0.187068194	1.047129035	Cytoplasm	Transcription regulator
Unnamed protein product	0.648634374		0.471870601	2.089296103	0.307609707	1.355188966	unknown	Other
SMEK homolog 2	0.625172675		0.450730801	2.108628035	0.299226493	1.318256974	unknown	Other
Unnamed protein product	0.625172675	0.003137056	0.454783201	2.108628035	0.299226493	1.318256974	Cytoplasm	Other
Gonadotrophin alpha 1 subunit	0.625172675	0.035022072	0.778641701	1.29419601	0.291071713	0.809095919	Extracellular space	Other
Follicle stimulating hormone beta subunit	0.619441092	0.045384203	0.358060092	1.380383968	0.383707315	0.855066717	Extracellular space	Other
Hypothetical protein LOC335859	0.586138189		0.409159511	2.108628035	0.280543387	1.235947013	Cytoplasm	Enzyme
Dynactin subunit 2	0.529663384	0.019913448	0.269459903	1.570363045	0.017701089	0.831763685	Cytoplasm	Other
Melanin concentrating hormone 2 (MCH2) precursor	0.510505021	0.189016216	0.694045424	1.940886021	0.27289781	0.990831971	Extracellular space	Other
60S acidic ribosomal protein P2	0.428548515		0.27934891	2.108628035	0.205116197	0.90364939	Cytoplasm	Other
Rho GDP-dissociation inhibitor 1	0.398107201	0.127483736	0.273517191	2.290868044	0.021086279	0.912010789	Cytoplasm	Other
Hypothetical protein LOC569455	0.325087309		0.216371298	2.108628035	0.154170096	0.685488224	Nucleus	Transporter
Growth hormone 2	0.207014099	0.076665109	0.229496703	2.398833036	0.098174803	0.496592313	Extracellular space	Cytokine
Somatolactin (alpha)	0.1458814	0.06390252	6.09E-05	3.311311007	0.046989411	0.48305881		

reagents and MS/MS in the amago salmon pituitary, treated (or not) with excess GH1.

In the iTRAQ-MS/MS analysis, we identified 1178 unique proteins (confidence > 95%) from 26,800 spectra; 569 unique proteins at the 5% FDR threshold level. Additionally, by the statistical analysis performed using the ProteinPilot 3.0 software, we defined 63 unique proteins that exhibited differential expression (≥1.25-fold change) in pituitaries cultured with excess GH1.

In order to understand the function of the differentially expressed proteins, we used the IPA software to classify these proteins according to their subcellular localizations, molecular functions, and biological functions. In this analysis, because the fish protein database is not rich in functional information compared to databases for human and mouse, we used BLAST to cross-reference the differentially expressed proteins with their counterparts in the human non-redundant protein database. Among the 63 unique proteins, 61 were identified as having human homologs.

First, these 61 differentially expressed proteins were classified into five discrete subcellular localization categories (cytoplasm, nucleus, plasma membrane, extracellular space, and other). About half of the differentially expressed proteins (59.0%) are localized to the cytoplasm (Fig. 1A).

Second, we classified the 61 proteins into the following eight categories based on their molecular function: enzyme, transporter, peptidase, transcription regulator, cytokine, kinase, translation regulator, and other. Among the 61 proteins, 52.5% of the differentially expressed proteins were classified into multiple categories; 39.4% were classified in single categories as either enzyme (14.8%), transporter (13.1%), peptidase (6.6%) or transcriptional regulation (4.9%) (Fig. 1B).

Third, we classified the proteins based on their biological function ontology. This analysis revealed that many of the proteins that are differentially expressed in response to excess GH1 treatment are molecules related to endocrine systems, cell growth and proliferation, and metabolism (Fig. 1C).

3.1.1. *Endocrine systems*

Fig. 2 indicates the expression levels of peptide hormones in the excess GH1-treated pituitary. In this study, although the expression of endogenous GH1 did not change in response to excess GH1 treatment, levels of the paralogous GH2 decreased; those data suggest that GH2 expression in the amago salmon pituitary is suppressed by excess GH1 treatment.

Another pituitary hormone, somatolactin (SL), which belongs to the GH/PRL family, has been identified only in fishes. SL has two isoforms (SLA and SLB), which are expressed in different sites within the pituitary [28]. Although SL plays important roles in growth, reproduction and metabolism, the functional difference (if any) between SLA and SLB remains unclear. In the proteome analysis, the expression level of SLA, but not SLB, decreased markedly in the GH1-treated pituitary; those data suggest that the two isoforms of SL might be differently regulated by excess GH1 treatment, just as GH1 and GH2 are. However, it is still not clear how differences in expression levels among isoforms of GH and SL affect physiological functions in salmon.

In contrast, two isoforms (PRL1 and PRL2) of PRL, a peptide hormone belonging to GH family, were increased in the excess GH1-treated pituitary (Fig. 2). PRL stimulates increases in food intake and body weight [4]. PRL2 is expressed only in fish, and its function has been postulated to be similar to that of PRL [29]. Up-regulation of both PRL1 and PRL2 in the pituitary in response to excess GH1 treatment might be involved in enhancement of food intake and increase of body weight.

Proteome analysis indicated that glycoprotein hormone FSH, consisting of an α-subunit (CGA) and β-subunit (FSHB), was also decreased in the excess GH1-treated pituitary (Fig. 2). FSH is a major regulator of gonadal development, and is required for oogenesis in females and spermatogenesis in males. Further, inhibition of the FSH receptor induces abnormalities in ovogenesis and spermatogenesis in salmon [6]. Thus, the down-regulation of FSH in the pituitary by excess GH1 treatment might induce attenuation of gonadal development and abnormal fertility. Furthermore, CGA is a subunit of another pituitary glycoprotein hormone, TSH and LH, whose β-subunits are TSHB and LHB, respectively [1,2]. Therefore, down-regulation of CGA by excess GH1 treatment might affect formation and functions of TSH and LH even though levels of LHB and TSHB do not change.

The expression levels of proteins related to hormone production of pituitary also changed in response to excess GH1 treatment (Table 2). PHD finger protein 17 (PHF17) is an E3 ubiquitin ligase that targets β-catenin for proteasomal degradation [30]. β-Catenin is a major component of cell–cell adherence junctions; in the pituitary, it plays a role in cellular organization and cell–cell signaling, which are important for production and secretion of pituitary hormone [31]. Therefore, in the excess GH1-treated pituitary, up-regulation of PHF17 might influence production and secretion of pituitary hormone via the disruption of the pituitary cell network, mediated by downregulation of β-catenin.

Calcium/calmodulin-dependent protein kinase II γ (CAMK2G) is one component of calcium/calmodulin-dependent kinase II (Ca/CAMK II), and plays a key role as a calcium signaling mediator in various tissues, including the pituitary. In the pituitary, Ca/CAMK II increases the mRNA expression level of some pituitary hormones [32,33]. Thus, down-regulation of CAMK2G would presumably affect the expression levels of these hormones (Table 2). Proprotein convertase subtilisin/kexin type 1 (PCSK1), which is expressed in brain and endocrine organs including pituitary, plays a major role in proteolytic cleavage of peptide hormones (e.g., POMC) and neuropeptide precursors. PCSK1 null mice and humans with loss-of-function PCSK1 mutations exhibit multiple endocrine defects [34,35]. Thus, in the excess GH1-treated pituitary, down-regulation of PCSK1 might lead to multiple endocrine defects as a result of impaired hormone processing (Table 2).

Taken together, the balance and regulation of various hormones in the pituitary were influenced by excess GH1 treatment. The induced imbalance of pituitary hormones might affect the regulation of many biological and physiological functions in excess GH1-treated salmon.

3.1.2. *Cell growth and cell proliferation*

In our proteome analysis, we investigated differential expression dynamics of proteins, including metabolic enzymes, ribosomal proteins, and proliferation related proteins, in the excess GH1-treated pituitary. Aldolase C (ALDOC), triosephosphate isomerase 1 (TPI1), and glyceraldehyde-3-phosphate dehydrogenase (GAPDH) are enzymes of the glycolytic pathway, involved in the conversion of glucose into lactate or pyruvate. Mitochondrial

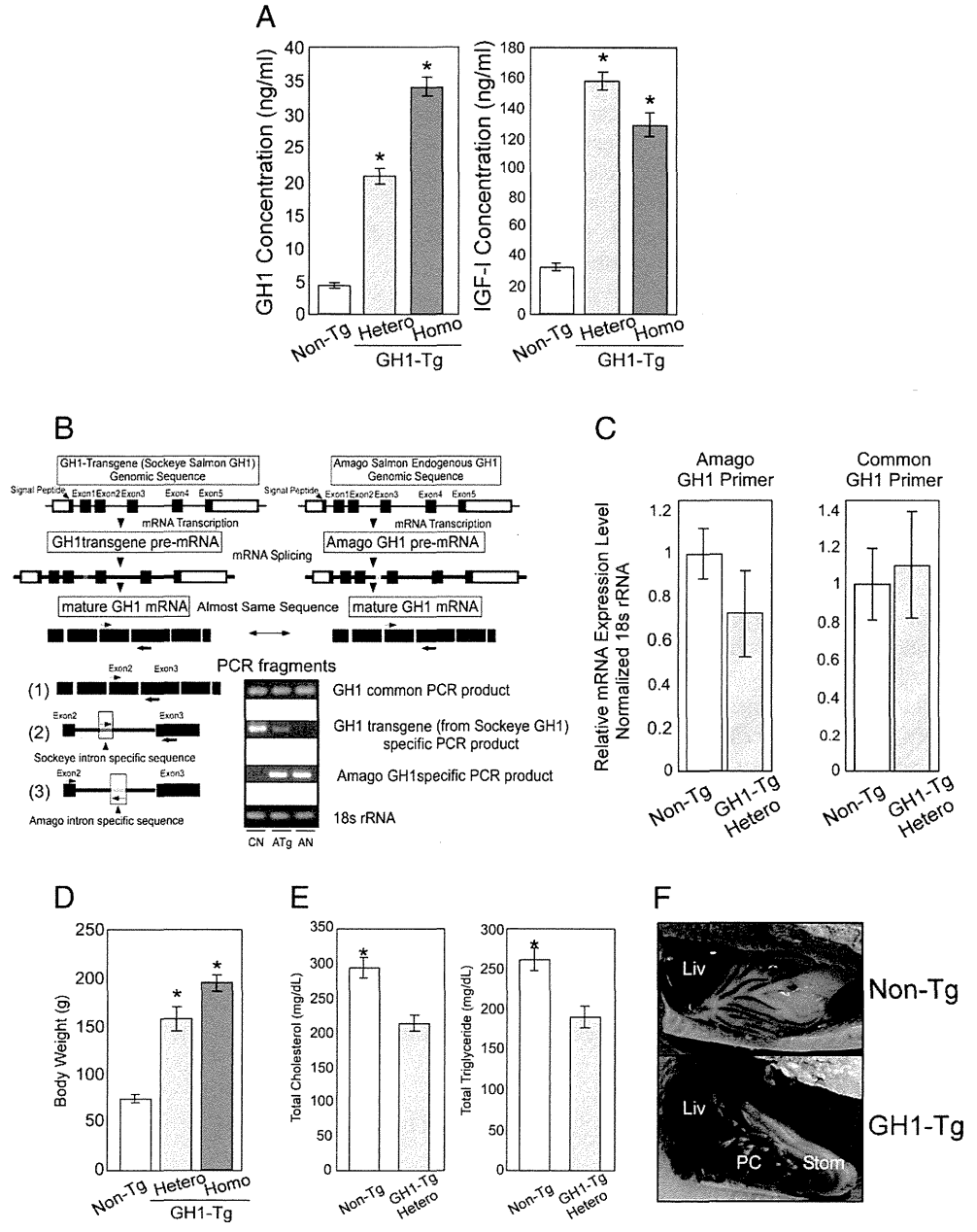

Fig. 3 – Characteristics of transgenic amago salmon overexpressing type 1 growth hormone (GH1). (A) The concentration of GH1 and IGF-I in plasma. GH1 and IGF-I levels in plasma were determined by ^{125}I-based radioimmuno assay. (B) Exon–intron structure of GH1-transgene (sockeye salmon) and amago salmon GH1 gene. To distinguish between amago salmon endogenous GH1 gene and sockeye salmon transgenic GH1 gene, primer sets used in reverse transcription (RT) PCR were designed against the region between exon 2 and exon 3, as follows: (1) GH1 common primers, which amplify both genes; (2) GH1 transgene-specific primers, which amplify only the sockeye salmon transgenic GH1 gene; and (3) amago-specific primers, which amplify only the endogenous amago salmon GH1 gene, respectively. CN, ATg, and AN indicated non-Tg coho salmon (*Oncorhynchus kisutch*), GH1-Tg amago salmon integrated sockeye salmon GH1 gene, and non-Tg amago salmon, respectively. Coho salmon DNA was also used for positive control to GH1 transgene-specific (the sockeye salmon transgenic GH1) primers and negative control to amago-specific primers. (C) GH1 mRNA levels in the pituitary, determined by qRT-PCR using primer sets (1) and (3) described in Fig. 3B. (D) Comparison of body weights among GH1-Tg (homo- and heterozygous) amago and non-Tg amago. (E) Total cholesterol and triglyceride concentrations in plasma derived from GH1-Tg heterozygotes and non-Tg amago. (F) Representative visceral fat of non-Tg (top) and GH1-Tg heterozygous (bottom) amago. "Liv", "PC", and "Stom" indicate liver, pyloric caeca, and stomach, respectively. Asterisks denoted significant differences between non-Tg and GH1-Tg amago at $p < 0.05$ by one-way ANOVA (A, D) or Student's t-test (C, E).

ATP synthase subunit β (ATP5B) is a catalytic core subunit of mitochondrial membrane ATP synthase, and plays a crucial role of mitochondrial oxidative phosphorylation (OXPHOS). In comparison with proliferating cells, quiescent cells exhibit a decrease in expression of glycolytic enzymes and an increase in expression of OXPHOS related enzymes [36–38]. In this study, we observed down-regulation of ALDOC, TPI1, and GAPDH, and up-regulation of ATP5B in the excess GH1-treated pituitary (Table 2). Reduction of ribosomal protein also causes attenuation of cell proliferation [39,40]. In the excess GH1-treated pituitary, 60S ribosomal protein P2 (RPLP2) and L24 (RPL24) were decreased (Table 2). Furthermore, an increase in ubiquitin-specific peptidase 7 (USP7), which is a deubiquitinating enzyme and stabilizes various proteins like p53, MDM2 p53-binding protein, and RE1-silencing transcription factor, is predicted to induce a reduction in cell proliferation and differentiation [41–43]. Inhibition of apoptosis inducing factor 1 (AIFM1), a flavoprotein with an oxidoreductase enzymatic activity, would induce cell cycle arrest and the suppression of cell proliferation [44]. A decrease in cold-inducible RNA-binding protein (CIRBP), an RNA-binding protein involved in a variety of stress response and disease processes in various cell types, would induce a reduction in cell proliferation, viability, and stress response ability [45,46]. The expression level of prothymosin α (PTMA), a nuclear acidic protein, is correlated to proliferation activity in a pituitary cell line (GH1 cell) [47]. In the excess GH1-treated pituitary, up-regulation of USP7 and down-regulation of AIFM1, CIRBP, and PTMA were detected (Table 2). Thus, our results suggest that GH1 treatment might cause cell cycle arrest and the suppression of cell proliferation in the salmon pituitary.

3.1.3. *Lipid metabolism*

In the excess GH1-treated pituitary, the expression levels of malic enzyme 3 (ME3) and fatty acid synthase (FASN), which are lipid metabolism-related enzymes, were altered. ME3 catalyzes the conversion of malate to pyruvate, producing NADPH [48]. FASN plays a role in *de novo* biogenesis of long-chain fatty acids via utilization of NADPH [49]. Thus, up-regulation of ME3 and down-regulation of FASN in the excess GH1-treated pituitary suggest that excess GH1 treatment induces cells to suppress lipid synthesis (Table 2).

3.2. *Protein profile in the GH1 transgenic salmon*

3.2.1. *Characteristics of GH1 transgenic salmon*

To confirm that protein dynamics in the excess GH1-treated pituitary are the same as those *in vivo*, we generated a GH1-Tg amago salmon. The GH1 transgene, consisting of a sockeye salmon GH1 gene under the control of the metallothionein B (MT-B) promoter, was integrated into the amago salmon genome, resulting in over-expression of GH1 throughout the whole body. In the plasma of GH1-Tg amago salmon (both homo- and heterozygous), the concentrations of GH1 and GH1-induced IGF-I were markedly elevated (Fig. 3A). To investigate the expression level of GH1 in the pituitary of GH1-Tg amago salmon, we performed qRT-PCR analysis using three primer sets: (1) GH1 common primer, (2) GH1 transgene (from sockeye salmon) specific primer, and (3) endogenous GH1 (from amago salmon) specific primer (Fig. 3B), which can detect a total GH1, GH1 from the transgene, and endogenous GH1, respectively (Fig. 3B). qRT-PCR analysis using these primer sets indicated that, in the pituitary, GH1 transgenesis has an insignificant effect on total of GH1, because endogenous GH1 expression is down-regulated by *in vivo* GH1 regulation system that is activated by the increase in the level of transgenic GH1 (Fig. 3C). However, GH1 transgenesis had a variety of effects on the phenotypes of GH1-Tg amago salmon. Compared to non-Tg amago salmon, the average body weights of heterozygous and homozygous GH1-Tg individual were ~2- and 3-

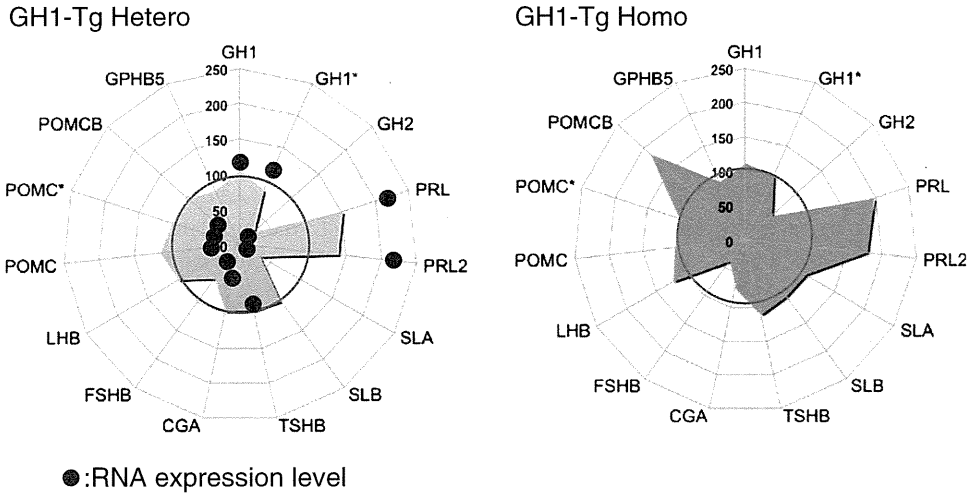

Fig. 4 – Comparison of expression levels of pituitary hormones in the GH1-Tg (homo- and heterozygous) and non-Tg pituitary by proteome and transcriptome analysis. Blue and red charts show that expression levels of pituitary hormones detected by proteome analysis in the pituitary of GH1-Tg (homo- and heterozygous). Asterisks indicate isoforms of identical pituitary hormones. Red circles indicate expression levels of pituitary hormones in non-Tg pituitary. Blue dots indicate expression levels of pituitary hormones obtained from subtractive microarray analysis. Each level represents the average among spots corresponding to each hormone gene. GH1/GH2 and PRL/PRL2 have highly similar sequences within each pair.

fold larger, respectively (Fig. 3D). In addition, GH1-Tg amago salmon exhibited enhancement of feeding behavior, shrinkage of the pituitary, and reduction of fertility, as do other GH1-Tg fish [5,17,50]. Furthermore, levels of total triglyceride and total cholesterol in the plasma of GH-Tg amago salmon were significantly decreased (Fig. 3E). Moreover, GH1-Tg amago salmon exhibited a reduction in visceral fat (Fig. 3F). These phenotypes were consistent with changes in protein expression levels observed in the excess GH1-treated pituitary.

3.2.2. *Identification of proteins and genes expressed in the GH1-Tg pituitary*

Proteins expressed specifically in the GH1-Tg pituitary were investigated by iTRAQ-MS/MS, resulting in the identification of 86 unique proteins that exhibit differential expression (≥1.25-fold change) in the GH1-Tg homozygous and/or heterozygous pituitary. Among them, 50 proteins did not change in the pituitary in response to excess GH1 treatment; 36 proteins were differentially regulated in excess GH1-treated pituitary. In the 36 proteins, the expression of the 28 proteins in the GH1-Tg homozygous and/or heterozygous pituitary showed similar pattern of the expression compared with excess GH1-treated pituitary, however, the expression of the remaining 8 proteins showed opposite expression pattern compared with that of excess GH1 treatment (Supplementary Table 1). The change in hormone balance in the GH1-Tg pituitary was almost identical to what was observed in the excess GH1-treated pituitary, except that SLA level did not change in the pituitary of the GH1-Tg homozygote (Figs. 2 and 4).

Additionally, we prepared customized amago salmon-specific subtractive microarrays using 1920 sequences (1915 amago cDNAs and 5 control DNAs). From the microarray analysis of mRNA levels in the pituitary, 45 genes (148 spots) listed in Supplementary Table 2 exhibited significant changes in the GH1-Tg amago heterozygote (fold change >1.5, $p<0.05$). The GH-Tg pituitary exhibited up-regulation of PRL/PRL2 and down-regulation of GH2, SLA, CGA and FSHB, just as in the excess GH1-treated pituitary; the mRNA levels of POMC and POMCB were markedly down-regulated (Fig. 4). These results were consistent with the down-regulation of GH gene expression in the pituitary from GH1-Tg salmon [50]. Bioinformatic analysis suggested that most of these differentially regulated molecules are involved in endocrine systems, metabolism, cell growth and proliferation (Supplementary Fig. 2).

4. Conclusion

In this study, excess GH1 treatment induced differential expression of pituitary proteins involved in endocrine systems, metabolism, cell proliferation and growth. In addition, the same protein dynamics were observed in the pituitary of GH1-Tg amago salmon. Furthermore, the characteristics predicted from these protein dynamics corresponded to the phenotypes of GH1-Tg salmon; these include enhancement of somatic growth and feeding behavior, shrinkage of the pituitary, reduction of fertility, and imbalances of lipid metabolism. Based on the results described above, we hypothesize that the regulation of hormone production and lipid metabolism are important to the enhancement of salmon somatic growth in response to GH1 treatment for the purpose of productivity improvement.

Supplementary materials related to this article can be found online at doi:10.1016/j.jprot.2011.12.009.

Acknowledgments

We are grateful to Dr. Hironori Ando for the technical advice about pituitary organ culture and to Dr. Koichiro Kano and Dr. Yoshinao Oki for IPA support. This work was supported in part by the Special Coordination Funds for Promoting Science and Technology "Creation of Innovation Centers for Advanced Interdisciplinary Research Areas" (to H.H.) and in part by the special subsidies for private school of Japan 14360104 (to T.M.) and Japanese grants 17380120 (to T.M. and H.H.) from the Ministry of Education, Culture, Sports, Science, and Technology, Japan.

REFERENCES

[1] Weltzien FA, Norberg B, Helvik JV, Andersen Ø, Swanson P, Andersson E. Identification and localization of eight distinct hormone-producing cell types in the pituitary of male Atlantic halibut (*Hippoglossus hippoglossus* L.). Comp Biochem Physiol A Mol Integr Physiol 2003;134:315–27.
[2] Ooi GT, Tawadros N, Escalona RM. Pituitary cell lines and their endocrine applications. Mol Cell Endocrinol 2004;228:1–21.
[3] Breves JP, Seale AP, Helms RE, Tipsmark CK, Hirano T, Grau EG. Dynamic gene expression of GH/PRL-family hormone receptors in gill and kidney during freshwater-acclimation of Mozambique tilapia. Comp Biochem Physiol A Mol Integr Physiol 2011;158:194–200.
[4] Ben-Jonathan N, Hugo ER, Brandebourg TD, LaPensee CR. Focus on prolactin as a metabolic hormone. Trends Endocrinol Metab 2006;17:110–6.
[5] Sundström LF, Devlin RH, Johnsson JI, Biagi CA. Vertical position reflects increased feeding motivation in growth hormone transgenic coho salmon (*Oncorhynchus kisutch*). Ethology 2003;109:701–12.
[6] Sambroni E, Abdennebi-Najar L, Remy JJ, Le Gac F. Delayed sexual maturation through gonadotropin receptor vaccination in the rainbow trout *Oncorhynchus mykiss*. Gen Comp Endocrinol 2009;164:107–16.
[7] Wong AO, Zhou H, Jiang Y, Ko WK. Feedback regulation of growth hormone synthesis and secretion in fish and the emerging concept of intrapituitary feedback loop. Comp Biochem Physiol A Mol Integr Physiol 2006;144:284–305.
[8] Agellon LB, Davies SL, Lin CM, Chen TT, Powers DA. Rainbow trout has two genes for growth hormone. Mol Reprod Dev 1988;1:11–7.
[9] Mori T, Deguchi F, Ueno K. Differential expression of Gh1 and Gh 2 genes by competitive RT-PCR in rainbow trout pituitary. Gen Comp Endocrinol 2001;123:137–43.
[10] Melmed S. Acromegaly pathogenesis and treatment. J Clin Invest 2009;119:3189–202.
[11] Perrini S, Laviola L, Carreira MC, Cignarelli A, Natalicchio A, Giorgino F. The GH/IGF1 axis and signaling pathways in the muscle and bone: mechanisms underlying age-related skeletal muscle wasting and osteoporosis. J Endocrinol 2010;205:201–10.
[12] Rius-Francino M, Acerete L, Jiménez-Amilburu V, Capilla E, Navarro I, Gutiérrez J. Differential effects on proliferation of GH and IGFs in sea bream(*Sparus aurata*) cultured myocytes. Gen Comp Endocrinol 2011;172:44–9.

[13] Madsen K, Friberg U, Roos P, Edén S, Isaksson O. Growth hormone stimulates the proliferation of cultured chondrocytes from rabbit ear and rat rib growth cartilage. Nature 1983;304:545–7.
[14] Johnsson Jorgen I, Bjornsson Bjorn Th. Growth hormone increases growth rate, appetite and dominance in juvenile rainbow trout, *Oncorhynchus mykiss*. Anim Behav 1994;48:177–86.
[15] Devlin RH, Sakhrani D, Tymchuk WE, Rise ML, Goh B. Domestication and growth hormone transgenesis cause similar changes in gene expression in coho salmon (*Oncorhynchus kisutch*). Proc Natl Acad Sci USA 2009;106: 3047–52.
[16] Devlin RH, Biagi CA, Yesaki TY. Growth, viability and genetic characteristics of GH transgenic coho salmon strains. Aquaculture 2004;236:607–32.
[17] Rahman MA, Mak R, Ayad H, Smith A, Maclean N. Expression of a novel piscine growth hormone gene results in growth enhancement in transgenic tilapia (*Oreochromis niloticus*). Transgenic Res 1998;7:357–69.
[18] Sheridan MA. Effects of thyroxin, cortisol, growth hormone, and prolactin on lipid metabolism of coho salmon, *Oncorhynchus kisutch*, during smoltification. Gen Comp Endocrinol 1986;64:220–38.
[19] Krasnov A, Agren JJ, Pitäknen TI, Mölsä H. Transfer of growth hormone (GH)transgenes into Arctic charr. (*Salvelinus alpinus* L.) II. Nutrient partitioning in rapidly growing fish. Genet Anal 1999;15:99–105.
[20] Falcón J, Besseau L, Fazzari D, Attia J, Gaildrat P, Beauchaud M, et al. Melatonin modulates secretion of growth hormone and prolactin by trout pituitary glands and cells in culture. Endocrinology 2003;144:4648–58.
[21] Shilov IV, Seymour SL, Patel AA, Loboda A, Tang WH, Keating SP, et al. The Paragon Algorithm, a next generation search engine that uses sequence temperature values and feature probabilities to identify peptides from tandem mass spectra. Mol Cell Proteomics 2007;6:1638–55.
[22] Tang WH, Shilov IV, Seymour SL. Nonlinear fitting method for determining local false discovery rates from decoy database searches. J Proteome Res 2008;7:3661–7.
[23] Mori T, Hiraka I, Kurata Y, Kawachi H, Mano N, Devlin RH, et al. Changes in hepatic gene expression related to innate immunity, growth and iron metabolism in GH-transgenic amago salmon (*Oncorhynchus masou*) by cDNA subtraction and microarray analysis, and serum lysozyme activity. Gen Comp Endocrinol 2007;151:42–54.
[24] Shimizu M, Swanson P, Fukada H, Hara A, Dickhoff WW. Comparison of extraction methods and assay validation for salmon insulin-like growth factor-I using commercially available components. Gen Comp Endocrinol 2000;119:26–36.
[25] Swanson P. Radioimmunoassay of fish growth hormone, prolactin, and somatolactin. In: Hochachka PW, Mommsen TP, editors. Analytical Techniques. Biochemistry and Molecular Biology of Fishes. Amsterdam: Elsevier Inc; 1994. p. 545–56.
[26] Moriyama S, Swanson P, Nishii M, Takahashi A, Kawauchi H, Dickhoff WW, et al. Development of a homologous radioimmunoassay for coho salmon insulin-like growth factor-I. Gen Comp Endocrinol 1994;96:149–61.
[27] Mori T, Kawachi H, Imai C, Sugiyama M, Kurata Y, Kishida O, et al. Identification of a novel uromodulin-like gene related to predator-induced bulgy morph in anuran tadpoles by functional microarray analysis. PLoS One 2009;4:e5936.
[28] Jiang Q, Ko WK, Lerner EA, Chan KM, Wong AO. Grass carp somatolactin: I. Evidence for PACAP induction of somatolactin-alpha and -beta gene expression via activation of pituitary PAC-I receptors. Am J Physiol Endocrinol Metab 2008;295:E463–76.
[29] Manzon LA. The role of prolactin in fish osmoregulation: a review. Gen Comp Endocrinol 2002;125:291–310.
[30] Chitalia VC, Foy RL, Bachschmid MM, Zeng L, Panchenko MV, Zhou MI, et al. Jade-1 inhibits Wnt signalling by ubiquitylating beta-catenin and mediates Wnt pathway inhibition by pVHL. Nat Cell Biol 2008;10:1208–16.
[31] Waite E, Lafont C, Carmignac D, Chauvet N, Coutry N, Christian H, et al. Different degrees of somatotroph ablation compromise pituitary growth hormone cell network structure and other pituitary endocrine cell types. Endocrinology 2010;151:234–43.
[32] Haisenleder DJ, Burger LL, Aylor KW, Dalkin AC, Marshall JC. Gonadotropin-releasing hormone stimulation of gonadotropin subunit transcription: evidence for the involvement of calcium/calmodulin-dependent kinase II (Ca/CAMKII) activation in rat pituitaries. Endocrinology 2003;144:2768–74.
[33] Wong AO, Li W, Leung CY, Huo L, Zhou H. Pituitary adenylate cyclase-activating polypeptide (PACAP) as a growth hormone (GH)-releasing factor in grass carp. I. Functional coupling of cyclic adenosine 3′,5′-monophosphate and Ca2+/calmodulin-dependent signaling pathways in PACAP-induced GH secretion and GH gene expression in grass carp pituitary cells. Endocrinology 2005;146:5407–24.
[34] Zhu X, Zhou A, Dey A, Norrbom C, Carroll R, Zhang C, et al. Disruption of PC1/3 expression in mice causes dwarfism and multiple neuroendocrine peptide processing defects. Proc Natl Acad Sci USA 2002;99:10293–8.
[35] Jackson RS, Creemers JW, Ohagi S, Raffin-Sanson ML, Sanders L, Montague CT, et al. Obesity and impaired prohormone processing associated with mutations in the human prohormone convertase 1 gene. Nat Genet 1997;16:303–6.
[36] López-Ríos F, Sánchez-Aragó M, García-García E, Ortega AD, Berrendero JR, Pozo-Rodríguez F, et al. Loss of the mitochondrial bioenergetic capacity underlies the glucose avidity of carcinomas. Cancer Res 2007;67:9013–7.
[37] Vander Heiden MG, Cantley LC, Thompson CB. Understanding the Warburg effect: the metabolic requirements of cell proliferation. Science 2009;324:1029–33.
[38] Cai Z, Zhao JS, Li JJ, Peng DN, Wang XY, Chen TL, et al. A combined proteomics and metabolomics profiling of gastric cardia cancer reveals characteristic dysregulations in glucose metabolism. Mol Cell Proteomics 2010;9: 2617–28.
[39] Chen A, Kaganovsky E, Rahimipour S, Ben-Aroya N, Okon E, Koch Y. Two forms of gonadotropin-releasing hormone (GnRH) are expressed in human breast tissue and overexpressed in breast cancer: a putative mechanism for the antiproliferative effect of GnRH by down-regulation of acidic ribosomal phosphoproteins P1 and P2. Cancer Res 2002;62:1036–44.
[40] Barna M, Pusic A, Zollo O, Costa M, Kondrashov N, Rego E, et al. Suppression of Myc oncogenic activity by ribosomal protein haploinsufficiency. Nature 2008;456: 971–5.
[41] Li M, Chen D, Shiloh A, Luo J, Nikolaev AY, Qin J, et al. Deubiquitination of p53 by HAUSP is an important pathway for p53 stabilization. Nature 2002;416:648–53.
[42] Li M, Brooks CL, Kon N, Gu W. A dynamic role of HAUSP in the p53-Mdm2 pathway. Mol Cell 2004;13:879–86.
[43] Huang Z, Wu Q, Guryanova OA, Cheng L, Shou W, Rich JN, et al. Deubiquitylase HAUSP stabilizes REST and promotes maintenance of neural progenitor cells. Nat Cell Biol 2011;13: 142–52.
[44] Schulthess FT, Katz S, Ardestani A, Kawahira H, Georgia S, Bosco D, et al. Deletion of the mitochondrial flavoprotein apoptosis inducing factor(AIF) induces

beta-cell apoptosis and impairs beta-cell mass. PLoS One 2009;4:e4394.
[45] Artero-Castro A, Callejas FB, Castellvi J, Kondoh H, Carnero A, Fernández-Marcos PJ, et al. Cold-inducible RNA-binding protein bypasses replicative senescence in primary cells through extracellular signal-regulated kinase 1 and 2 activation. Mol Cell Biol 2009;29:1855–68.
[46] Zeng Y, Kulkarni P, Inoue T, Getzenberg RH. Down-regulating cold shock protein genes impairs cancer cell survival and enhances chemosensitivity. J Cell Biochem 2009;107:179–88.
[47] Alvarez CV, Zalvide JB, Cancio E, Dieguez C, Regueiro BJ, Vega FV, et al. Regulation of prothymosin alpha mRNA levels in rat pituitary tumor cells. Neuroendocrinology 1993;57:1048–56.
[48] DeBerardinis RJ, Lum JJ, Hatzivassiliou G, Thompson CB. The biology of cancer: metabolic reprogramming fuels cell growth and proliferation. Cell Metab 2008;7:11–20.
[49] Menendez JA, Lupu R. Fatty acid synthase and the lipogenic phenotype in cancer pathogenesis. Nat Rev Cancer 2007;7:763–77.
[50] Mori T, Devlin RH. Transgene and host growth hormone gene expression in pituitary and nonpituitary tissues of normal and growth hormone transgenic salmon. Mol Cell Endocrinol 1999;149:129–39.

THE JOURNAL OF BIOLOGICAL CHEMISTRY VOL. 287, NO. 22, pp. 18710–18716, May 25, 2012

Structural Basis for Inhibition of Xyloglucan-specific Endo-β-1,4-glucanase (XEG) by XEG-Protein Inhibitor*

Received for publication, February 7, 2012 and in revised form, April 9, 2012 Published, JBC Papers in Press, April 10, 2012, DOI 10.1074/jbc.M112.350520

Takuya Yoshizawa (吉澤 拓也)[‡], Toshiyuki Shimizu (清水 敏之)[§], Hisashi Hirano (平野 久)[‡], Mamoru Sato (佐藤 衛)[‡], and Hiroshi Hashimoto (橋本 博)[‡1]

From the [‡]Graduate School of Nanobioscience, Yokohama City University, 1-7-29 Suehiro-cho, Tsurumi-ku, Yokohama, Kanagawa 230-0045, Japan and the [§]Graduate School of Pharmaceutical Science, The University of Tokyo, 7-3-1 Hongo, Bunkyo-ku, Tokyo 113-0033, Japan

Background: Plants produce glycoside hydrolase inhibitor protein to protect cell walls.
Results: The inhibition mechanism for a xyloglucanase-inhibitor of a fungal xyloglucanase is revealed by crystal structures.
Conclusion: Xyloglucanase inhibitor protein distinguishes specific structural features of a glycosyl hydrolase to protect the plant cell wall from degradation.
Significance: Understanding the mechanism of xyloglucanase inhibition is key to comprehending how plants defend themselves against microbes that express glycosyl hydrolases.

Microorganisms such as plant pathogens secrete glycoside hydrolases (GHs) to digest the polysaccharide chains of plant cell walls. The degradation of cell walls by these enzymes is a crucial step for nutrition and invasion. To protect the cell wall from these enzymes, plants secrete glycoside hydrolase inhibitor proteins (GHIPs). Xyloglucan-specific endo-β-1,4-glucanase (XEG), a member of GH family 12 (GH12), could be a great threat to many plants because xyloglucan is a major component of the cell wall in most plants. Understanding the inhibition mechanism of XEG by GHIP is therefore of great importance in the field of plant defense, but to date the mechanism and specificity of GHIPs remain unclear. We have determined the crystal structure of XEG in complex with extracellular dermal glycoprotein (EDGP), a carrot GHIP that inhibits XEG. The structure reveals that the conserved arginines of EDGP intrude into the active site of XEG and interact with the catalytic glutamates of the enzyme. We have also determined the crystal structure of the XEG-xyloglucan complex. These structures show that EDGP closely mimics the XEG-xyloglucan interaction. Although EDGP shares structural similarity to a wheat GHIP (*Triticum aestivum* xylanase inhibitor-IA (TAXI-IA)) that inhibits GH11 family xylanases, the arrangement of GH and GHIP in the XEG-EDGP complex is distinct from that in the xylanase-TAXI-IA complex. Our findings imply that plants have evolved structures of GHIPs to inhibit different GH family members that attack their cell walls.

Plant cell walls are composed of various polysaccharides such as cellulose, hemicellulose, and pectin. In most plant cell wall models, cellulose microfibrils are linked via hemicellulose. This cellulose-hemicellulose network provides tensile strength and acts as a physical barrier against microorganisms such as invading pathogens. To penetrate and utilize plant cell walls nutritionally, microorganisms secrete hydrolases for cell wall degradation. These enzymes, which include endoglucanases, xylanases, and polygalacturonases, are classified into glycoside hydrolase (GH)[2] families in the CAZY data base (1). In response to pathogenic attack, plants produce glycoside hydrolase inhibitor proteins (GHIPs) against the cell wall-degrading enzymes (2, 3).

Extracellular dermal glycoprotein (EDGP) from carrot is one such GHIP. EDGP shows inhibitory activity toward the xyloglucan-specific endo-β-1,4-glucanase (XEG) from the fungus *Aspergillus aculeatus* (4). EDGP is alternatively called XEG inhibitor protein (XEGIP). XEG belongs to GH family 12 (GH12) and specifically cleaves xyloglucan, which consists of a β-linked glucose backbone substituted with xylose side chains (5). Xyloglucan is a major hemicellulose in most plants (6), and thus xyloglucanases such as XEG are a great threat to plants because the degradation of hemicellulose causes great damage. The inhibition of XEG by EDGP is an important component of the plant defense system. Proteins homologous to EDGP have been identified in various plants, and several of these proteins have been characterized. Tomato XEGIP inhibits XEG by forming an associated 1:1 complex (7). Tobacco Necturin IV (NEC IV) also inhibits XEG (8). In contrast, the homologous protein from wheat, TAXI-IA (*Triticum aestivum* xylanase inhibitor-IA), inhibits a GH family 11 (GH11) xylanase from fungus, ANXI (*Aspergillus niger* xylanase I) (9–11). Interestingly, the homologous protein from soybean, basic 7S globulin (Bg7S), lacks inhibitory activity for either GH11 or GH12 enzymes (12).

* This work was supported by a Grant-in-Aid for Scientific Research (KAKENHI), the National Project on Protein Structural and Functional Analyses Protein 3000 Project, and the Targeted Proteins Research Program from Ministry of Education, Culture, Sports, Science, and Technology in Japan (MEXT) (to T. S., M. S., and H. H.).

The atomic coordinates and structure factors (codes 3VL8, 3VL9, 3VLA, and 3VLB) have been deposited in the Protein Data Bank, Research Collaboratory for Structural Bioinformatics, Rutgers University, New Brunswick, NJ (http://www.rcsb.org/).

[1] To whom correspondence should be addressed. Tel.: 81-45-508-7227; Fax: 81-45-508-7365; E-mail: hash@tsurumi.yokohama-cu.ac.jp.

[2] The abbreviations used are: GH, glycoside hydrolase; ANXI, *Aspergillus niger* xylanase I; Bg7S, basic 7S globulin; EDGP, extracellular dermal glycoprotein; GHIP, GH inhibitor protein; IL, inhibition loop; PDB, Protein Data Bank; TAXI-IA, *Triticum aestivum* xylanase inhibitor-IA; XEG, xyloglucan-specific endo-β-1,4-glucanase; XEGIP, XEG inhibitor protein; FI-CMCase, FI-carboxymethyl cellulose.

The crystal structures of the ANXI-TAXI-IA complex and Bg7S have been determined (10, 12). However, not only the inhibition mechanism of XEG but also the mechanism underlying family-specific inhibition by GHIP have remained unclear.

In this work, we have determined the crystal structures of XEG, the XEG-xyloglucan complex, EDGP, and the XEG-EDGP complex. The structure of the XEG-xyloglucan complex provides a structural basis of specific recognition of xyloglucan by XEG. The structure of the XEG-EDGP complex reveals how GHIP recognizes the active site of GH12 and inhibits its activity. Surprisingly, the arrangement of GH and GHIP in the XEG-EDGP complex is distinct from that in the ANXI-TAXI-IA complex. Our findings clarify the mechanism of family-specific inhibition of GH12 and GH11 by EDGP homologous GHIPs.

EXPERIMENTAL PROCEDURES

Preparation of EDGP and XEG—The preparation of EDGP and XEG has been described previously (12, 13). In brief, EDGP was purified from carrot callus culture medium. The carrot callus was grown for 2–3 weeks at 298 K in Murashige-Skoog medium containing 1 mg/liter 2,4-dichlorophenoxyacetic acid. The protein was purified using HiTrap SP (GE Healthcare). The cDNA encoding XEG was obtained by PCR-based gene synthesis (14) and inserted into pGEX6P-I vector (GE Healthcare) at the BamHI-XhoI site. N-terminal GST-fused XEG was expressed in *Escherichia coli* BL21. The protein was purified using glutathione-Sepharose 4B resin (GE Healthcare), a HiTrap Q HP column (GE Healthcare), and a HiLoad Superdex 75 26/60 column (GE Healthcare).

Enzyme Activity Assay—The activity of XEG wild-type or mutants was measured using *p*-hydroxybenzoic acid hydrazide (PAHBAH) method (15). The reaction mixture contained 50 mM sodium acetate, pH 4.6, 100 mM NaCl, 5 mg/ml xyloglucan from tamarind seeds (DS Pharma), and 100 ng of XEG in the absence or presence of 5 μg of EDGP. The final reaction volume was 20 μl. The reaction mixtures were incubated at room temperature for 15 min, and then the amount of reducing sugar was measured.

Crystallographic Analyses—All crystals were obtained by the hanging-drop vapor diffusion method at 293 K. Hexagonal crystals of XEG were obtained under 0.1 M sodium acetate, pH 5.5, and 1.5 M ammonium sulfate. The co-crystal of XEG-xyloglucan was obtained under 0.1 M sodium acetate, pH 4.6, 25% PEG 3000, and 5 mg/ml digested xyloglucan. XEG used in crystallization with xyloglucan was wild type. The preparation of digested xyloglucan has been described previously (16). Hexagonal crystals of EDGP were obtained under 0.2 M ammonium acetate, 0.1 M sodium acetate, pH 4.6, and 30% PEGMME2000. Iodine-derived crystals of EDGP were prepared by the vaporizing iodine labeling method (17). A droplet of iodine solution (0.67 M KI and 0.47 M I_2) was placed next to the crystallization droplet containing EDGP crystals. After 20 min, the iodine solution was removed and the crystallization droplet was incubated for a further 20 h.

To crystallize the XEG-EDGP complex, XEG protein with an N-terminal truncation, XEG(8–224), was prepared. The XEG-EDGP complex was prepared by mixing EDGP and XEG(8–224) in an equal molar ratio. Monoclinic crystals of the XEG-EDGP complex were obtained under 0.24 M Morpheus alcohols (Molecular Dimensions), 0.1 M Morpheus Buffer system 3, pH 8.5 (Molecular Dimensions), 30% Morpheus EOD_P8K (Molecular Dimensions), and 9% dextran sulfate.

X-ray diffraction data for crystals of XEG, XEG-xyloglucan, EDGP native, EDGP derivative, and XEG-EDGP were collected in-house at UltraX18 (Rigaku), Photon Factory (PF) BL-17A, SPring-8 BL-41XU, PF NE-3A, and SPring-8 BL-32XU, respectively. All diffraction data were processed using the program HKL2000 (18). The XEG structure was solved by the molecular replacement method with the program MOLREP (19) using the endo-β-1,4-glucanase from *Hypocrea jecorina* as a search model (Protein Data Bank (PDB) ID code 1OA2). The EDGP structure was solved by the SIRAS method using the programs SOLVE and RESOLVE (20). The EDGP-XEG complex structure was solved by the molecular replacement method with the program MOLREP (19) using EDGP and XEG structures as search models. Model building was performed with the program COOT (21). Structure refinement was performed with the programs CNS (22) and REFMAC (23). The geometries of the final structures were validated with the program PROCHECK (24). Data collection and refinement statistics are given in Table 1. Final coordinates and structure factors have been deposited in the Protein Data Bank Japan (PDBj).

Pulldown Assay—GST-fused XEG and its mutants were overexpressed in *E. coli* BL21 and purified by glutathione-Sepharose 4B resin. Next, EDGP and GST-fused XEG were incubated with glutathione-Sepharose 4B beads equilibrated with a buffer containing 50 mM sodium acetate, pH 4.6, and 100 mM NaCl for 1 h at 25 °C. The beads were washed with the above buffer and eluted with a buffer containing 100 mM Tris-HCl, pH 9.0, 200 mM NaCl, and 50 mM reduced glutathione. The GST tags were cleaved by HRV3C protease. The proteins in solution were analyzed by SDS-PAGE with Coomassie Brilliant Blue staining. Band intensities were calculated by the program ImageJ (National Institutes of Health).

Figure Preparation—Protein structures were prepared with the program PyMOL (DeLano Scientific). All of the figures were modified with the programs PHOTOSHOP and ILLUSTRATOR (Adobe Systems).

RESULTS

Structure of XEG-Xyloglucan Complex—We determined the crystal structures of XEG and XEG in complex with xyloglucan at 1.9 and 1.2 Å resolution, respectively. The structure of XEG bound to xyloglucan could be superimposed on that of XEG, with a root mean square deviation value of 0.6 Å for comparable Cα atoms. XEG adopts a β-jelly roll fold, as observed in other enzymes of the family GH12 (25). A cleft runs across the surface of the protein, and the xyloglucan-binding subsites are located within this cleft. The hydrolysis reaction of the GH12 enzymes proceeds with a two-step retaining mechanism catalyzed by two glutamate residues: one acts as the nucleophile and the other as the acid/base (25). The putative nucleophile and acid/base in XEG are Glu^{119} and Glu^{205}, respectively. The electron density map clearly shows binding of xyloglucan within the cleft, where the β-1,4-glucose backbone is bound to the −1 to

TABLE 1
Data collection and refinement statistics

Parameters	XEG	XEG-xyloglucan	EDGP	EDGP deriv	XEG-EDGP
Data collection					
Wavelength (Å)	1.5418	1.0000	0.8000	1.900	1.0000
Space group	$P6_5$	$P2_12_12_1$	$P6_2$	$P6_2$	$C2$
a (Å)	93.0	62.6	130.1	130.1	249.0
b (Å)	93.0	79.3	130.1	130.1	51.7
c (Å)	62.0	80.4	44.5	44.5	143.2
α (°)	90	90	90	90	90
β (°)	90	90	90	90	122.2
γ (°)	120	90	120	120	90
Resolution (Å)	50.0–1.90	50.0–1.20	50–0.92	50.0–2.40	50.0–2.70
Observed reflections	134,050	743,148	1,283,262	343,185	121,934
Unique reflections	24,103	120,607	272,047	16,855	40,308
R-merge (%)	8.3 (31.6)	6.9 (31.7)	7.5 (32.6)	6.4 (21.8)	7.8 (38.4)
Completeness (%)	99.6 (98.8)	95.8 (75.2)	91.6 (74.3)	98.2 (95.2)	91.9 (83.2)
$<I>/\sigma<I>$	14.8 (7.0)	12.8 (3.3)	12.2 (2.0)	19.2 (11.3)	12.4 (3.3)
Refinement					
Resolution (Å)	1.90	1.20	0.95		2.70
Refined reflections	22,833	114,328	239,679		37,707
Free reflections	1,142	5,716	11,983		1,885
R (%)	18.0	12.3	12.6		25.2
R-free (%)	21.2	16.2	14.5		33.9
Root mean square deviation					
Bond length (Å)	0.005	0.015	0.016		0.015
Bond angles (°)	0.951	1.637	1.782		1.823
Ramachandran plot					
Most favored (%)	93.7	92.7	89.3		82.3
Additional allowed (%)	5.8	7.3	10.1		16.4
Generously allowed (%)	0.5	0.0	0.3		0.8
Disallowed (%)	0.0	0.0	0.3		0.5
Protein Data Bank ID code	3VL8	3VL9	3VLA		3VLB

−4 subsites, and α-1,6-xylose residues branching from the glucose moieties in subsites −2 and −3 are also observed in the electron density (Fig. 1*A*). Trp^{13} and Trp^{28} form hydrophobic interactions with the glucose moieties of the β-1,4-glucan chain in the −4 and −2 subsites, respectively (Fig. 1*B*). In addition to these hydrophobic interactions, the catalytic Glu^{119} and Glu^{205} residues form hydrogen bonds with oxygen atoms of the glucose moiety in the −1 subsite.

The XEG structure shows the structural basis for specific recognition of xyloglucan by the enzyme. Tyr^{24} stacks against the xylose side chain linked to the glucose moieties in the −3 subsite, and Glu^{201} interacts with the O5 oxygen atoms of xylose (Fig. 1*B*). To investigate which residues are responsible for XEG activity, we prepared XEG mutants and measured their xyloglucanase activity (Fig. 1*C*). An XEG mutant with a W13A, W28A, or W13A/W28A substitution(s) lacked almost all xyloglucanase activity, clearly indicating that these tryptophans, which are involved in the hydrophobic interaction with the glucose backbone, are essential for this activity. Remarkably, a Y24A substitution also markedly decreased the activity of XEG. Tyr^{24} of XEG is not conserved in the GH12 enzyme from *A. aculeatus*, FI-CMCase (26). FI-CMCase hydrolyzes carboxylmethylated β-1,4-glucan, a model substrate of cellulase, and cleaves xyloglucan with approximately half of the activity of XEG. These results suggest that a stacking interaction of a hydrophobic nature between Tyr^{24} and the xylose side chain is crucial for xyloglucan recognition. A previous study has revealed the crystal structure of a GH12 xyloglucanase from *Bacillus licheniformis* (BlXG12) in complex with xyloglucan (27). In this structure, tryptophan residues are involved in interactions with glucose backbone just as we observe with XEG. However, stacking interactions between an aromatic residue and a xylose residue were not observed. This is consistent with the fact that the BlXG12 also possesses glucanase activity to digest carboxymethyl cellulose (CMC) (27).

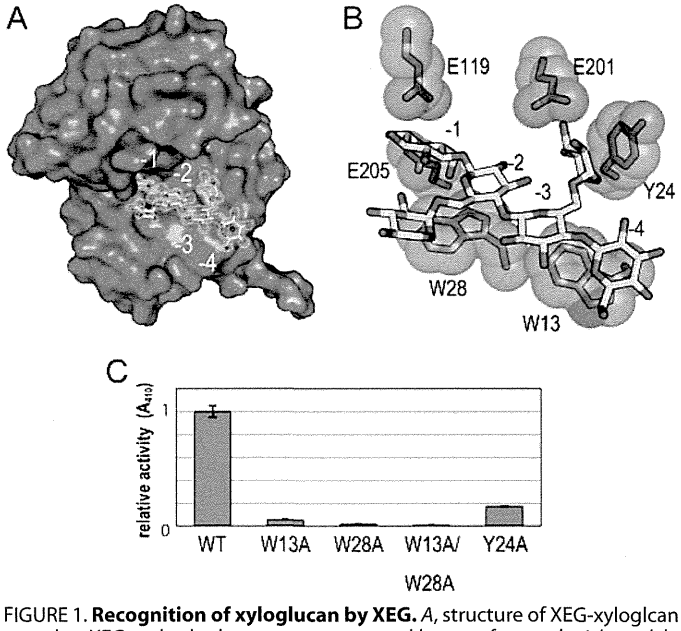

FIGURE 1. **Recognition of xyloglucan by XEG.** *A*, structure of XEG-xyloglcan complex. XEG and xyloglucan are represented by a *surface* and *stick models*, respectively. The observed electron density of xyloglucan is shown by *white mesh* ($2F_o - F_c$, 1σ). *B*, detailed interactions between XEG and xyloglucan are shown by *stick* and *sphere models*. Carbon of XEG, carbon of xyloglucan, oxygen, and nitrogen are colored *light blue*, *yellow*, *red*, and *blue*, respectively. *C*, activities of the XEG mutants were estimated relative to that of wild-type (*WT*).

Structure of EDGP—The crystal structure of carrot EDGP was determined at 0.95 Å resolution (Fig. 2*A*). In the structure, the N-terminal glutamine is converted to a pyroglutamic acid

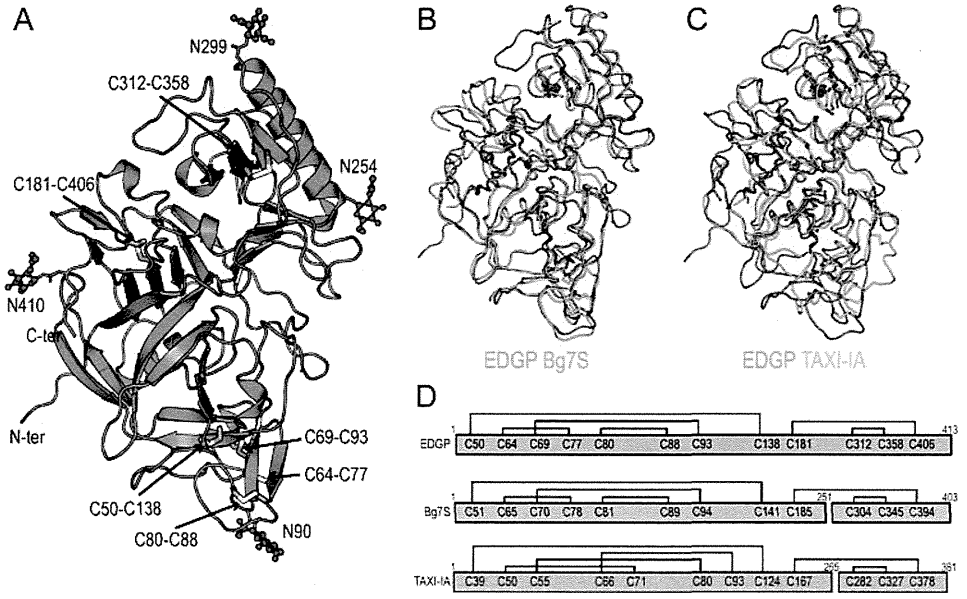

FIGURE 2. **Crystal structure of EDGP.** *A*, overall structure of EDGP is represented by a *ribbon model*. The disulfide bonds are shown by *stick models*, in which sulfur atoms are colored *yellow*. *N*-Linked glycans are represented by *ball* and *stick models* and colored *red*. *B*, superimposed structures of EDGP (*orange*) and Bg7S (*light green*) are represented as *wire models*. *C*, superimposed structures of EDGP (*orange*) and TAXI-IA (*cyan*) are represented as *wire models*. *D*, schematic drawing shows disulfide bonds in EDGP, Bg7S, and TAXI-IA.

(28). EDGP adopts a pepsin-like fold that is β-rich with several α-helices and is roughly divided by a center cleft comprising the active site (29). Despite the structural similarity to pepsin, one of the catalytic aspartates in pepsin is replaced by Ser^{271} in EDGP, and thus EDGP lacks protease activity. Consistent with this, other GHIPs also lack the catalytic aspartate. EDGP has six disulfide bonds, and these supposedly stabilize the tertiary structure of EDGP in the extracellular environment (Fig. 2, *A* and *D*). EDGP has four putative *N*-linked glycosylation sites: Asn^{90}, Asn^{254}, Asn^{299}, and Asn^{410} (28). In each putative *N*-linked glycosylation site, the electron density map indicated at least one sugar moiety linked to the asparagine (Fig. 2*A*).

The crystal structures of homologous proteins from wheat (TAXI-IA) and soybean (Bg7S) have been reported previously (10, 12). The overall structure of EDGP is similar to those of Bg7S and TAXI-IA. The root mean square deviation value for Cα atoms comparable with Bg7S (PDB ID code 3AUP) and TAXI-IA (PDB ID code 1T6E) is 1.6 and 2.4 Å, respectively (Fig. 2, *B* and *C*). EDGP, Bg7S, and TAXI-IA all have six disulfide bonds. Although the patterns of disulfide formation are conserved in EDGP and Bg7S, they differ from that in TAXI-IA (Fig. 2*D*). Bg7S and TAXI-IA undergo post-translational cleavage in their internal regions, whereas EDGP does not (Fig. 2*D*). The variation in post-translational modification of GHIPs is of interest, although the functional associations of these modifications in GHIPs remains unclear.

Structure of XEG-EDGP Complex, and Its Interaction—The crystal structure of XEG in complex with EDGP was determined at 2.7 Å resolution (Fig. 3*A*). The XEG-EDGP complex structure shows that EDGP completely covers the active cleft of XEG. The averaged root mean square deviations of comparable Cα atoms between each native structure (XEG and EDGP) and the XEG-EDGP complex are 0.8 and 0.7 Å, respectively, suggesting no substantial conformational changes occur in EDGP upon the binding of XEG. The calculated buried solvent-accessible surface area is 2046 $Å^2$ in the complex, comparable with that of the ANXI-TAXI-IA complex (1998 $Å^2$). We did not observe sugar chains at all of the *N*-linked glycosylation sites of EDGP because of ambiguity in the electron density map. In the XEG-EDGP structure, Arg^{322} and Arg^{403} of EDGP insert into the active cleft of XEG and form an electrostatic interaction with the catalytic residues, Glu^{119} and Glu^{205} (Fig. 3*B*). Hydrophobic interactions are made between the aliphatic moiety of Arg^{403} of EDGP and Trp^{28} of XEG, Leu^{202} and Pro^{203} of EDGP and Trp^{13} of XEG (Fig. 3*B*). To identify the amino acid residues of XEG responsible for the interaction with EDGP, we performed a pulldown assay using XEG mutants and EDGP (Fig. 3*C*). We did not observe a marked reduction in the interaction with EDGP with single or double mutations. However, mutations in residues involved in the interaction with EDGP weakened the binding ability, suggesting that both electrostatic and hydrophobic interactions are important in the interaction between XEG and EDGP (Fig. 3, *B* and *C*).

Structural overlay of the XEG-EDGP inhibition complex and the XEG-xyloglucan complex revealed the strategy employed by EDGP for inhibition (Fig. 4). Namely, the guanidium moieties of Arg^{322} and Arg^{403} of EDGP in the inhibition complex are located in the −1 subsite of XEG, and the aliphatic moiety of the side chain of Arg^{403} is located in the −2 subsite of XEG. Furthermore, Leu^{202} and Pro^{203} of EDGP, which are conserved in most plants, are located in the −4 subsite of XEG. These findings indicate that EDGP mimics the interaction between XEG and xyloglucan observed in the structure of the XEG-xyloglucan complex. Interestingly, EDGP does not interact with Tyr^{24} of XEG, which is involved in xylose recognition (Fig. 1*B*). The lack of any interaction with Tyr^{24} of XEG might be explained by our unpublished data that EDGP also inhibits the glucanase activity of FI-CMCase, which lacks this tyrosine res-

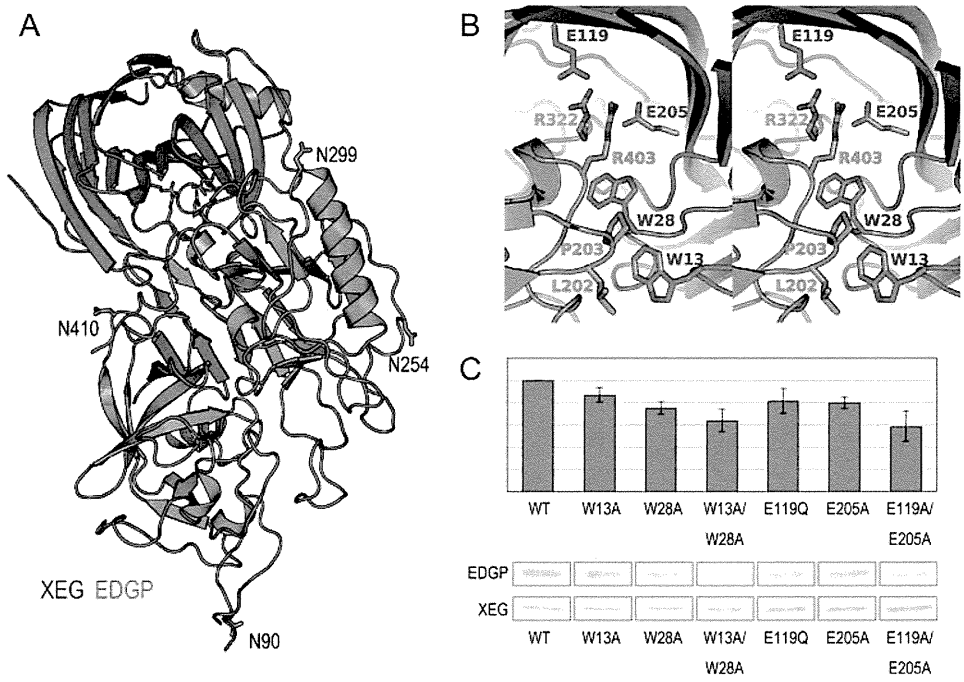

FIGURE 3. **Crystal structure of the XEG-EDGP inhibition complex and interactions between EDGP and XEG.** *A*, overall structure of inhibition complex of EDGP (*orange*) and XEG (*light blue*) shown by a *ribbon model*. *B*, stereo view of the detailed interactions between EDGP (*orange*) and XEG (*light blue*). *C*, binding activity of XEG mutants with EDGP (*upper panel*) estimated by band intensity of pulldown assay (*bottom panel*).

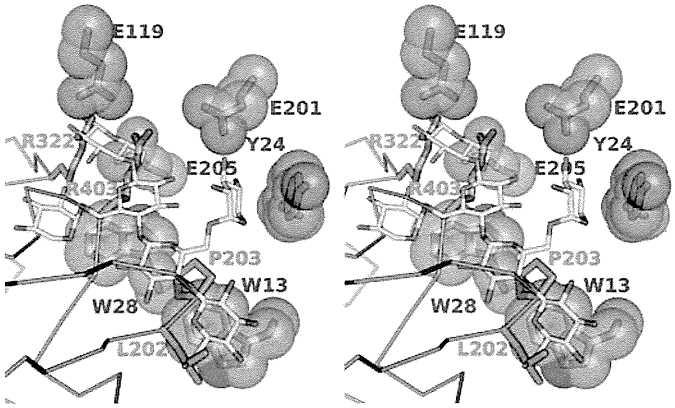

FIGURE 4. **Comparison between XEG-EDGP and XEG-xyloglucan interactions.** Stereo view shows XEG-EDGP interactions, with xyloglucan superimposed from the structure of XEG-xyloglucan. XEG (*light blue*), EDGP (*orange*), and xyloglucan (*yellow*) are shown by *stick and sphere*, *stick and wire*, and *stick models*, respectively.

idue. The EDGP complex with FI-CMCase has been crystallized (13) and solved.[3]

DISCUSSION

The crystal structure of the XEG-xyloglucan complex provides a structural basis for understanding the specific recognition of xyloglucan by XEG. The structure of the XEG-EDGP inhibition complex reveals details of the inhibition mechanism, in which two arginines located in inhibition loops 1 and 2 (IL-1 and IL-2) of EDGP intrude into the catalytic cleft of XEG and mimic the interactions formed between XEG and xyloglucan (Figs. 4 and 5*A*). The two arginines in IL-1 and IL-2 are conserved in most GHIPs, including homologous proteins from tomato, tobacco, potato, and *Arabidopsis* (Fig. 5*B*). Of these, tomato and tobacco GHIPs inhibit GH12 enzymes (7, 8). Furthermore, Leu^{202} and Pro^{203} (which contact the −4 subsite of the enzyme active site) are also conserved in GHIPs of most plants. Although the inhibitory activity of GHIP from potato or *Arabidopsis* has not been reported, our results suggest that these GHIPs might inhibit GH12 enzymes by means of their conserved arginines, leucine, and proline. In the GH11-TAXI-IA complex, Leu^{292} in IL-1 and His^{374} in IL-2 are involved in target-binding interactions. These residues are conserved in GHIPs of some monocots of the order Poales, including grasses, whose hemicellulose is xylan. Thus, rye GHIP might inhibit GH11 enzymes instead of GH12.

Structural overlays of EDGP and TAXI-IA in the GH-GHIP complexes reveal very similar positioning of IL-1 and IL-2 in these complexes (Fig. 5*A*), indicating that EDGP and TAXI-IA use similar regions to interact with their corresponding GHs. Although the overall structures of XEG and EDGP are comparable with those of ANXI and TAXI-IA (Fig. 2*C*), the arrangement of GH and GHIP in the XEG-EDGP complex is distinct from that in the ANXI-TAXI-IA complex (Fig. 5*C*). There is a small but significant difference between the XEG and ANXI structures. The structure of GH displaying the β-jelly roll fold including GH11 and GH12 has been likened to a right hand, with a thumb, palm, and fingers (30). The thumb or fingers forms a lid over the active site cleft in both ANXI and XEG (Fig. 5*C*). The putative model structure of an ANXI-EDGP or XEG-TAXI-IA complex built by superimposition of the GH structures clearly shows a steric clash between the lid of GH and GHIP (Fig. 5*D*). This indicates an intrinsic difference in the lid structures of ANXI and XEG which is conserved in each member of the GH11 and GH12 families. Therefore, our findings

[3] T. Yoshizawa, T. Shimizu, H. Hirano, M. Sato, and H. Hashimoto, unpublished data.

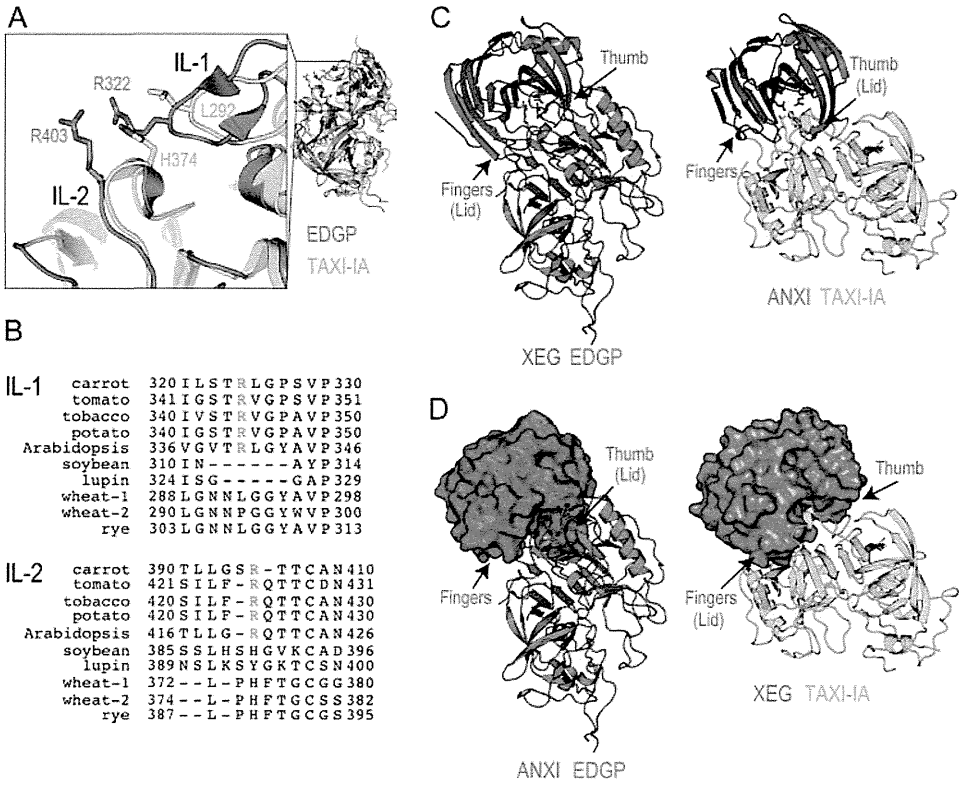

FIGURE 5. **Diverse mechanisms of target recognition of GH12 and GH11 by GHIP.** *A*, close-up view (*left*) around IL-1 and IL-2 of the superimposed structures (*right*) of EDGP (*orange*) and TAXI-IA (*cyan*). *B*, sequence alignment of IL-1 and IL-2 of EDGP with homologous proteins from various plants, tomato (UniProt ID; Q8GT67), tobacco (Q3KU27), potato (Q7XJE7), *Arabidopsis* (Q8LF70), soybean (P13917), lupin (Q42369), wheat-1 (Q8H0K8), wheat-2 (Q53IQ4), and rye (Q6KE41). Conserved arginines are colored *orange*. *C*, comparison of structures between XEG-EDGP (*left panel*) and ANXI-TAXI-IA (*right panel*). Complexes are represented by *ribbon models*. *D*, putative model structure of an ANXI-EDGP (*left panel*) or XEG-TAXI-IA (*right panel*) complex.

imply that plants have evolved structures of GHIPs to inhibit specific GH families of enzymes that attack their cell walls. In addition to TAXI, wheat has xylanase inhibitor protein I, which possesses two independent enzyme-binding sites and is able to inhibit both GH10 and GH11 xylanases (31). Plants employ related proteins and mechanisms for target recognition of GH to protect their cell walls using conserved patterns of interacting residues.

Acknowlegments—We thank the beamline staff of SPring-8 and PF for data collection and Dr. H. Shiota, Yokohama City University, for supplying carrot callus, and Dr. J. R. H. Tame, Yokohama City University for English corrections.

REFERENCES

1. Henrissat, B. (1991) A classification of glycosyl hydrolases based on amino acid sequence similarities. *Biochem. J.* **280,** 309–316
2. Juge, N. (2006) Plant protein inhibitors of cell wall degrading enzymes. *Trends Plant Sci.* **11,** 359–367
3. Lagaert, S., Beliën, T., and Volckaert, G. (2009) Plant cell walls: protecting the barrier from degradation by microbial enzymes. *Semin. Cell Dev. Biol.* **20,** 1064–1073
4. Shang, C., Sassa, H., and Hirano, H. (2005) The role of glycosylation in the function of a 48-kDa glycoprotein from carrot. *Biochem. Biophys. Res. Commun.* **328,** 144–149
5. Pauly, M., Andersen, L. N., Kauppinen, S., Kofod, L. V., York, W. S., Albersheim, P., and Darvill, A. (1999) A xyloglucan-specific endo-β-1,4-glucanase from *Aspergillus aculeatus*: expression cloning in yeast, purification and characterization of the recombinant enzyme. *Glycobiology* **9,** 93–100
6. Hayashi, T. (1989) Xyloglucans in the primary cell wall. *Annu. Rev. Plant Physiol. Plant Mol. Biol.* **40,** 139–168
7. Qin, Q., Bergmann, C. W., Rose, J. K., Saladie, M., Kolli, V. S., Albersheim, P., Darvill, A. G., and York, W. S. (2003) Characterization of a tomato protein that inhibits a xyloglucan-specific endoglucanase. *Plant J.* **34,** 327–338
8. Naqvi, S. M., Harper, A., Carter, C., Ren, G., Guirgis, A., York, W. S., and Thornburg, R. W. (2005) Nectarin IV, a potent endoglucanase inhibitor secreted into the nectar of ornamental tobacco plants: isolation, cloning, and characterization. *Plant Physiol.* **139,** 1389–1400
9. Gebruers, K., Brijs, K., Courtin, C. M., Fierens, K., Goesaert, H., Rabijns, A., Raedschelders, G., Robben, J., Sansen, S., Sørensen, J. F., Van Campenhout, S., and Delcour, J. A. (2004) Properties of TAXI-type endoxylanase inhibitors. *Biochim. Biophys. Acta* **1696,** 213–221
10. Sansen, S., De Ranter, C. J., Gebruers, K., Brijs, K., Courtin, C. M., Delcour, J. A., and Rabijns, A. (2004) Structural basis for inhibition of *Aspergillus niger* xylanase by *Triticum aestivum* xylanase inhibitor-I. *J. Biol. Chem.* **279,** 36022–36028
11. Fierens, K., Gils, A., Sansen, S., Brijs, K., Courtin, C. M., Declerck, P. J., De Ranter, C. J., Gebruers, K., Rabijns, A., Robben, J., Campenhout, S., Volckaert, G., and Delcour, J. A. (2005) His^{374} of wheat endoxylanase inhibitor TAXI-I stabilizes complex formation with glycoside hydrolase family 11 endoxylanases. *FEBS J.* **272,** 5872–5882
12. Yoshizawa, T., Shimizu, T., Yamabe, M., Taichi, M., Nishiuchi, Y., Shichijo, N., Unzai, S., Hirano, H., Sato, M., and Hashimoto, H. (2011) Crystal structure of basic 7S globulin, a xyloglucan-specific endo-β-1,4-glucanase inhibitor protein-like protein from soybean lacking inhibitory activity against endo-β-glucanase. *FEBS J.* **278,** 1944–1954
13. Yoshizawa, T., Shimizu, T., Hirano, H., Sato, M., and Hashimoto, H. (2011) Purification, crystallization and x-ray diffraction study of extracellular dermal glycoprotein from carrot and the inhibition complex that it forms with an endo-β-glucanase from *Aspergillus aculeatus*. *Acta Crystallogr. Sect. F Struct. Biol. Cryst. Commun.* **67,** 830–832

14. Hoover, D. M., and Lubkowski, J. (2002) DNAWorks: an automated method for designing oligonucleotides for PCR-based gene synthesis. *Nucleic Acids Res.* **30,** e43
15. Lever, M. (1972) A new reaction for colorimetric determination of carbohydrates. *Anal. Biochem.* **47,** 273–279
16. Martinez-Fleites, C., Guerreiro, C. I., Baumann, M. J., Taylor, E. J., Prates, J. A., Ferreira, L. M., Fontes, C. M., Brumer, H., and Davies, G. J. (2006) Crystal structures of *Clostridium thermocellum* xyloglucanase, XGH74A, reveal the structural basis for xyloglucan recognition and degradation. *J. Biol. Chem.* **281,** 24922–24933
17. Miyatake, H., Hasegawa, T., and Yamano, A. (2006) New methods to prepare iodinated derivatives by vaporizing iodine labelling (VIL) and hydrogen peroxide VIL (HYPER-VIL). *Acta Crystallogr. D Biol. Crystallogr.* **62,** 280–289
18. Otwinowski, Z., and Minor, W. (1997) Processing of x-ray diffraction data collected in oscillation mode. *Methods Enzymol.* **276,** 307–326
19. Vagin, A., and Teplyakov, A. (1997) MOLREP: an automated program for molecular replacement. *J. Appl. Crystallogr.* **30,** 1022–1025
20. Terwilliger, T. (2004) SOLVE and RESOLVE: automated structure solution, density modification and model building. *J. Synchrotron Radiat.* **11,** 49–52
21. Emsley, P., and Cowtan, K. (2004) COOT: model-building tools for molecular graphics. *Acta Crystallogr. D Biol. Crystallogr.* **60,** 2126–2132
22. Brünger, A. T., Adams, P. D., Clore, G. M., DeLano, W. L., Gros, P., Grosse-Kunstleve, R. W., Jiang, J. S., Kuszewski, J., Nilges, M., Pannu, N. S., Read, R. J., Rice, L. M., Simonson, T., and Warren, G. L. (1998) Crystallography & NMR system: a new software suite for macromolecular structure determination. *Acta Crystallogr. D Biol. Crystallogr.* **54,** 905–921
23. Murshudov, G. N., Vagin, A. A., and Dodson, E. J. (1997) Refinement of macromolecular structures by the maximum-likelihood method. *Acta Crystallogr. D Biol. Crystallogr.* **53,** 240–255
24. Laskowski, R. A., MacArthur, M. W., Moss, D. S., Thornton, J. M. (1993) PROCHECK: a program to check the stereochemical quality of protein structure. *J. Appl. Crystallogr.* **26,** 283–291
25. Sandgren, M., Ståhlberg, J., and Mitchinson, C. (2005) Structural and biochemical studies of GH family 12 cellulases: improved thermal stability, and ligand complexes. *Prog. Biophys. Mol. Biol.* **89,** 246–291
26. Kanda, T., Wakabayashi, K., and Nisizawa, K. (1976) Synergistic action of two different types of endocellulase components from *Irpex lacteus* (*Polyporus tulipiferae*) in the hydrolysis of some insoluble celluloses. *J Biochem.* **79,** 997–1005
27. Gloster, T. M., Ibatullin, F. M., Macauley, K., Eklöf, J. M., Roberts, S., Turkenburg, J. P., Bjørnvad, M. E., Jørgensen, P. L., Danielsen, S., Johansen, K. S., Borchert, T. V., Wilson, K. S., Brumer, H., and Davies, G. J. (2007) Characterization and three-dimensional structures of two distinct bacterial xyloglucanases from families GH5 and GH12. *J. Biol. Chem.* **282,** 19177–19189
28. Shang, C., Shibahara, T., Hanada, K., Iwafune, Y., and Hirano, H. (2004) Mass spectrometric analysis of posttranslational modifications of a carrot extracellular glycoprotein. *Biochemistry* **43,** 6281–6292
29. Browner, M. F., Smith, W. W., and Castelhano, A. L. (1995) Matrilysin-inhibitor complexes: common themes among metalloproteases. *Biochemistry* **34,** 6602–6610
30. Törrönen, A., Harkki, A., and Rouvinen, J. (1994) Three-dimensional structure of endo-1,4-β-xylanase II from *Trichoderma reesei*: two conformational states in the active site. *EMBO J.* **13,** 2493–2501
31. Payan, F., Leone, P., Porciero, S., Furniss, C., Tahir, T., Williamson, G., Durand, A., Manzanares, P., Gilbert, H. J., Juge, N., and Roussel, A. (2004) The dual nature of the wheat xylanase protein inhibitor XIP-I: structural basis for the inhibition of family 10 and family 11 xylanases. *J. Biol. Chem.* **279,** 36029–36037

JOURNAL OF PROTEOMICS 74 (2011) 431–441

available at www.sciencedirect.com

ScienceDirect

www.elsevier.com/locate/jprot

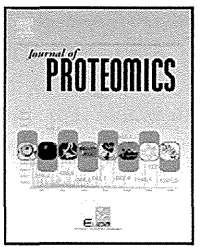

N^{α}-Acetylation of yeast ribosomal proteins and its effect on protein synthesis

Masahiro Kamita[a], *Yayoi Kimura*[a], *Yoko Ino*[a], *Roza M. Kamp*[b], *Bogdan Polevoda*[c], *Fred Sherman*[c], *Hisashi Hirano*[a,*]

[a]*Graduate School of Nanobioscience, Yokohama City University, Suehiro 1-7-29, Tsurumi, Yokohama 230-0045, Japan*
[b]*University of Applied Science and Technology, 13347 Berlin, Germany*
[c]*Department of Biochemistry and Biophysics, University of Rochester Medical Center, Rochester, NY 14642, USA*

ARTICLE INFO

Article history:
Received 21 November 2010
Accepted 15 December 2010
Available online 22 December 2010

Keywords:
N^{α}-Acetylation
Ribosome
Ribosomal protein
2D-DIGE

ABSTRACT

N^{α}-Acetyltransferases (NATs) cause the N^{α}-acetylation of the majority of eukaryotic proteins during their translation, although the functions of this modification have been largely unexplored. In yeast (*Saccharomyces cerevisiae*), four NATs have been identified: NatA, NatB, NatC, and NatD. In this study, the N^{α}-acetylation status of ribosomal protein was analyzed using NAT mutants combined with two-dimensional difference gel electrophoresis (2D-DIGE) and mass spectrometry (MS). A total of 60 ribosomal proteins were identified, of which 17 were N^{α}-acetylated by NatA, and two by NatB. The N^{α}-acetylation of two of these, S17 and L23, by NatA was not previously observed. Furthermore, we tested the effect of ribosomal protein N^{α}-acetylation on protein synthesis using the purified ribosomes from each NAT mutant. It was found that the protein synthesis activities of ribosomes from NatA and NatB mutants were decreased by 27% and 23%, respectively, as compared to that of the normal strain. Furthermore, we have shown that ribosomal protein N^{α}-acetylation by NatA influences translational fidelity in the presence of paromomycin. These results suggest that ribosomal protein N^{α}-acetylation is necessary to maintain the ribosome's protein synthesis function.

1. Introduction

Methionine cleavage and N^{α}-acetylation are two common protein N-terminal modifications [1,2]. A majority of experimentally characterized eukaryotic proteins are N-terminally acetylated by N^{α}-acetyltransferases (NATs) during their translation from mRNA [3]. In yeast (*Saccharomyces cerevisiae*), approximately 57% of proteins are predicted to have an N^{α}-acetyl group, while the corresponding figure for mammalian proteins is about 84% [4]. The N^{α}-acetylation is catalyzed by NATs that contain catalytic subunits homologous to the GNAT family of acetyltransferase [5]. In yeast, four NATs have been identified, NatA, NatB, NatC, and NatD, which are composed of the following catalytic and auxiliary subunits: Ard1p and Nat1p for NatA; Nat3p and Mdm20p for NatB; and Mak3p, Mak10p, and Mak31p for NatC [6]. A recent study has shown NatD to consist of only a catalytic subunit: Nat4p [7]. The deletion of NATs induces various phenotypes. The NatA deletion mutant exhibits defects in sporulation, salt sensitivity, mating efficiency, and the ability to enter G0. The NatB deletion mutant shows increased osmotic sensitivity, decreased utilization of non-fermentable carbon sources, reduced mating efficiency, inability to form functional actin filaments, defects in mitochondrial and vacuolar inheritance, random polarity, increased sensitivity to the anti-mitotic drugs, and increased susceptibility to a number of DNA damaging agents. The NatC deletion mutant shows a decreased growth on YPG medium at 37 °C, although growth on YPD medium at 30 °C is nearly normal [6].

* *Corresponding author.* Tel.: +81 45 508 7439; fax: +81 45 508 7667.
E-mail address: hirano@yokohama-cu.ac.jp (H. Hirano).

1874-3919/$ – see front matter © 2010 Elsevier B.V. All rights reserved.
doi:10.1016/j.jprot.2010.12.007

Despite the wide occurrence of protein N^{α}-acetylation, it is unknown how many proteins require N^{α}-acetylation for function. For instance, the N^{α}-acetylation of Orc1p and Sir3p was shown to be necessary for transcriptional silencing in yeast [8,9]. Also, the N^{α}-acetylation of the killer viral coat protein Gag by NatC is required for assembly and maintenance of the L-A dsRNA viral particle in yeast [10]. Unacetylated actin and tropomyosin have a number of defects *in vivo* and *in vitro*, although the mutants are viable [11]. While the N^{α}-acetylation of ribosomal proteins has been known for decades [12–14], the role of N^{α}-acetylation in translation has not been determined.

The ribosome is a large ribonucleoprotein complex that synthesizes proteins in the cytoplasm. The core of the structure, as well as many of the ribosomal functions, is highly conserved between eukaryotes and prokaryotes [15]. In yeast, the ribosome consists of two subunits, the large (60S) and small (40S) subunits. The 60S subunit is composed of three ribosomal RNAs (rRNAs) and 46 ribosomal proteins, whereas the 40S subunit is composed of one rRNA and 32 ribosomal proteins [16,17]. The ribosome translates mRNA sequences into the corresponding amino acids and links them together to synthesize proteins. There are four stages of protein synthesis: initiation, elongation, termination, and recycling [18]. The 60S subunit polymerizes the polypeptide chain during the elongation phase. The 40S subunit is associated with mRNA tracks, the tRNA binding site, and is instrumental in selecting an aminoacyl-tRNA that complements the bound mRNA codon [16]. Although the rRNAs basically catalyze translation of mRNA and peptide bond formation, ribosomal proteins have been shown to play several important roles in protein synthesis, including determining the conformation of the ribosome structure and binding the various translational factors [19].

The ribosomal proteins undergo a variety of post-translational modifications including phosphorylation, methylation, glycosylation, and N^{α}-acetylation (co-translational). The post-translational modifications are thought to affect the ribosomal function. For example, Ruvinsky et al. reported that phosphorylation of ribosomal protein S6 controls cell size and glucose homeostasis [20]. Phosphorylation of ribosomal protein P1A exerts an effect on the hetero-oligomerization process [21]. Additionally, it is known that arginine methylation of ribosomal protein S10 regulates ribosome biogenesis [22], and arginine methylation of ribosomal proteins S3 affects ribosome assembly [23]. Glycosylation of ribosomal proteins is required for aggregation of untranslated messenger ribonucleoproteins into stress granules [24]. Clearly, modifications of ribosomal proteins are important for protein synthesis. However, the effect of N^{α}-acetylation of ribosomal proteins, and therefore changes of ribosome function remain unknown.

In this study, we comprehensively analyzed ribosomal protein N^{α}-acetylation using NAT mutants combined with two-dimensional difference gel electrophoresis (2D-DIGE) and mass spectrometry (MS). These analyses led to the identification of 19 ribosomal proteins acetylated by NatA and NatB. Subsequently, we investigated the effect of ribosomal protein N^{α}-acetylation on protein synthesis using the NatA deletion mutant.

2. Material and methods

2.1. Yeast strains and media

The following strains were used in this study: the normal strain, B-8032 (MATα *ura3-52 CYC1-963 cyc7-67 lys5-10*); the *nat1* mutant, B-8360 (MATα *nat1::URA3 ura3-52 CYC1-963 cyc7-67 lys5-10*); the *mak3* mutant, B-9074 (MATα *mak3::URA3 CYC1-963 cyc7-67 lys5-10*); and the *nat3* mutant, B-11974 (MATα *nat3::kanMX2 CYC1-963 cyc7-67 lys5-10*).

The YPD medium [2% (w/v) glucose, 2% (w/v) pepton, and 1% (w/v) yeast extract] was used for growing yeast. To purify 80S ribosomes, the yeast cells were cultured in the YPD medium at 30 °C. The cells were grown to the mid log phase, an absorbance of ~2 A_{600}U/ml, and harvested by centrifugation, washed once with deionized water and stored at −80 °C. For the 10-fold serial dilution assays, freshly grown yeast colonies were suspended in deionized water, and 1/10 dilutions, starting at an optical density of 0.1 at 600 nm, were spotted on a YPD plate or a YPD plate containing antibiotics. The plates were then incubated at 20, 30, or 37 °C for 3 to 4 days.

2.2. Purification of 80S ribosomes and ribosomal proteins

Purification of yeast ribosomes was performed as described by Ulrich A et al. with some modifications [25]. Briefly, the stored yeast cells were resuspended in the extraction buffer [20 mM HEPES-KOH pH 7.0, containing 5 mM Mg-acetate$_2$, 2 mM spermidine, 0.1 mM EGTA, 10 mM 2-mercaptoethanol, 10% (v/v) glycerol, and 0.1 mM PMSF]. Glass beads were added and the cells broken by vigorous vortex shaking. The homogenate was centrifuged at 20,000 ×*g* for 30 min at 4 °C. To purify 80S ribosomes, the concentration of KCl in the supernatant was adjusted to 0.4 M while being mixed gently. Thereafter, the supernatant was centrifuged at 65,000 ×*g* for 5 h at 4 °C. The resulting ribosome pellet was then resuspended in the dissociation buffer [20 mM HEPES-KOH pH 7.0, containing 5 mM Mg-(Ac)$_2$, 500 mM K(Ac), 0.1 mM EGTA, 10 mM 2-mercaptoethanol, 10% (v/v) glycerol, and 0.1 mM PMSF] and puromycin and GTP were added to a final concentration of 1 mM each. The mixture was incubated at 30 °C for 30 min. After incubation, the ribosome was pelleted through a 25% (v/v) glycerol cushion in the dissociation buffer at 65,000 ×*g* for 12 h at 4 °C using a swinging bucket rotor. The pellet was resuspended again and then centrifuged at 65,000 ×*g* for 12 h at 4 °C. Finally, the resulting 80S ribosome pellet was resuspended in the reaction buffer [50 mM Tris–HCl pH 7.6 containing 15 mM $MgCl_2$, and 90 mM KCl]. To separate the ribosomal proteins from the rRNA of the ribosome, the resuspended pellet was precipitated with 0.1 volume of 0.1% (w/v) DTT, 0.1 volume of 1 M $MgCl_2$, and 2.5 volume of glacial acetic acid. After incubation on ice for 1 h, the rRNA was removed by centrifugation at 20,000 ×*g* for 10 min. The supernatant was dialyzed against deionized water.

2.3. Gel electrophoresis of rRNAs and ribosomal proteins

The rRNAs (1 μg) were incubated at 65 °C for 2 min in the loading solution [0.1% (w/v) SDS, 5% (v/v) glycerol and BPB],

and subjected to electrophoresis in 0.8% (w/v) agarose gel. The ribosomal proteins (10 μg) were incubated at 65 °C for 10 min in the sample buffer [0.05 M Tris–HCl pH 6.8, containing 2% (w/v) SDS, 5% (v/v) 2-mercaptoethanol, 10% (v/v) glycerol, and BPB] and subsequently separated by SDS-PAGE. On the other hand, two-dimensional electrophoresis (2-DE) was performed using acid-urea gels containing 8 M urea in the first dimension toward the cathode (pH 5.0) at constant 200 V for 800 Vh, and SDS-PAGE (14% acrylamide gel) in the second dimension. After 2-DE, proteins were detected by CBB R-250 staining.

2.4. *Two-dimensional difference gel electrophoresis*

For 2D-DIGE, purified ribosomal proteins were minimally labeled with CyDyes (GE Healthcare, Little Calfont, UK) Cy3 and Cy5 according to the manufacturer's protocol. Equal amounts of purified ribosomal proteins from the normal and the mutant strains were labeled with two different dyes, Cy3 for the normal and Cy5 for the mutant strains. The ratio of ribosomal proteins to CyDye was 50 μg to 128 pmol. All labeled samples were combined and dissolved in 20 μl of sample solution [10% (v/v) 2-mercaptoethanol, 10% (v/v) glycerol, 1% (v/v) acetic acid and 8 M urea], and was subjected to 2-DE. The separated proteins were detected using Typhoon 9400 (GE Healthcare).

2.5. *Protein identification by mass spectrometric analysis*

After electrophoresis, protein spots were cut from the gels, destained three times with destaining solution [50 mM NH_4HCO_3/60% ACN], and digested with trypsin in 50 mM NH_4HCO_3 at 37 °C for 12 h. The tryptic digests were applied to Amicon Ultrafree-MC (0.22 μm) devices and centrifuged at 7000 rpm for 5 min. After filtration, a solution containing 0.02% (v/v) TFA and 0.2% (v/v) formic acid was added to the Amicon Ultrafree-MC tubes and centrifuged again. The resulting peptides were resuspended in 0.3% (v/v) formic acid, and analyzed using an ESI-Linear Ion Trap (LIT)-TOF MS (NanoFrontier LD, Hitachi-High Technologies, Tokyo, Japan) or an ESI-Q-TOF MS (Micromass, Manchester, UK), respectively. For data analysis, the raw MS spectrum was processed using the Hitachi-High Technologies' data processing software or the Micromass' MassLynx software to generate MGF and PKL files, respectively. The obtained MS and MS/MS data were searched against the 6,858 yeast protein sequences of the SWISS-PROT ver. 57.4 database using the MASCOT program, ver. 2.2.04 (Matrix Science, London, UK) to identify proteins. The search parameters were as follows: protease digestion with two missed cleavages permitted, enzyme specificity was set to consider trypsin, propionamidation of cysteine, and oxdation of methionine as variable modifications, and mass tolerance was set to 0.5 Da for the fragment ions and precursor ions. The confidence interval for the MASCOT scores was set to 95% (significance threshold $p<0.05$). Additionally, search results that yielded a MASCOT score of ≥95 or 35 for SDS-PAGE or 2-DE, respectively, were accepted as positive identifications.

2.6. *Poly (U)-dependent poly (Phe) synthesis assay*

The 80S ribosomes (0.3 A_{260}U) from the normal and the mutant strains were incubated in 25 μl of an assay mixture containing 50 μg of S-100 fraction, which was purified from the normal strain, 15 μg of polyuridylic acid, 25 μg of tRNA, [^{14}C]-phenylalanine, 0.5 mM GTP, 1 mM ATP, 2 mM phosphocreatine, and 40 μg/ml creatine phosphokinase in 50 mM Tris–HCl pH 7.6, 15 mM $MgCl_2$, 90 mM KCl, and 5 mM 2-mercaptoethanol at 30 °C for 30 min. After incubation, samples were precipitated with 10% (w/v) trichloroacetic acid (TCA) and boiled for 10 min. Subsequently, the samples were placed on ice for 10 min and filtered through glass fiber filters. The filters were washed twice with 10% (w/v) TCA. After air-drying, the insoluble proteins were resuspended in 10% (w/v) TCA and the radioactivity was measured using a liquid scintillation counter.

2.7. *Polysome profiles*

Yeast cells were grown to a mid log phase in the YPD medium. The cells were harvested in the presence of 100 μg/ml cycloheximide for 10 min. Preparation of yeast extracts was carried out by glass bead disruption in 10 mM Tris–HCl pH 7.4, containing 100 mM NaCl, 30 mM $MgCl_2$, and 100 μg/ml cycloheximide. A 200 μl sample of lysate, corresponding to 8 A_{260} U, was applied to a 7–47% linear sucrose gradient that was prepared in 50 mM Tris–acetate pH 7.0, containing 50 mM NH_4Cl, 30 mM $MgCl_2$ and 1 mM DTT for 2.5 h at 38,200 rpm (Beckman, SW40Ti). After centrifugation, fractions were collected from top to bottom with continuous A_{254} monitoring.

2.8. *Translational fidelity assay*

The reporter assay described by Liang et al. was performed with slight modifications [26]. Briefly, a 366 bp PCR fragment containing the Protein A gene was amplified from the common TAP tag. To create the gene encoding the FLAG tag, which is immediately downstream from the stop codon gene of protein A, the first PCR fragment was used as a template for the second PCR. The created PCR fragment was inserted into the KpnI and XbaI restriction site in the plasmid pAUR123. The construct was transformed into both the normal strain and the *nat1* mutant. The transformed cells were disrupted using YPER buffer (Pierce, Rockford, IL, USA) and glass beads. Cell extracts were centrifuged at 20,000 ×*g* for 10 min at 4 °C and supernatants analyzed by SDS-PAGE. The separated proteins were transferred to a polyvinylidene difluoride (PVDF) membrane and the protein A peptide on the membrane was detected with anti-peroxidase antibody. The membrane was incubated with ECL plus (GE Healthcare) and the positive signals were detected using an LAS4000 illuminator (Fuji Film, Tokyo, Japan).

3. Results

3.1. *Ribosome purification and ribosomal protein identification by two-dimensional electrophoresis*

In this study, we purified the 80S ribosomes from the normal yeast strain and the NAT mutants. To check the quality of the purified 80S ribosomes, rRNAs and ribosomal proteins were separated by standard gel electrophoresis (Fig. 1A). As shown in Fig. 1A, sharp bands of 25S and 18S rRNAs were detected, while no